Targeting p38 MAPK signaling pathway: Quercetin as a novel therapy for TMJ synovitis

MOSHA CHENG[1*], YUHE GUAN[1*], XIAOTAO XIN[2], XIN YI[3] and YI LIU[4]

[1]Department of Oral and Maxillofacial Surgery, School and Hospital of Stomatology, China Medical University, Liaoning Provincial Key Laboratory of Oral Disease, Shenyang, Liaoning 110002, P.R. China; [2]Department of Stomatology, First Affiliated Hospital of Jinzhou Medical University, Jinzhou, Liaoning 121001, P.R. China; [3]Department of Oral Anatomy and Physiology, School and Hospital of Stomatology, China Medical University, Liaoning Provincial Key Laboratory of Oral Disease, Shenyang, Liaoning 110002, P.R. China; [4]School and Hospital of Stomatology, China Medical University, Liaoning Provincial Key Laboratory of Oral Disease, Shenyang, Liaoning 110002, P.R. China

Received July 14, 2025; Accepted August 27, 2025

DOI: 10.3892/ijmm.2025.5692

Abstract. Temporomandibular joint (TMJ) synovitis is a chronic inflammatory condition prevalent in temporomandibular disorders, characterized by synovial inflammation and bone degradation. Quercetin, a natural flavonoid with diverse bioactive properties, is investigated for its potential in ameliorating TMJ synovitis by targeting the p38 MAPK pathway. Using network pharmacology and *in vitro* and *in vivo* models, the effects of quercetin on synoviocytes and inflammatory responses were evaluated. Results showed quercetin's significant inhibition of synoviocyte proliferation, promotion of apoptosis and reduction of inflammatory cytokines. Moreover, quercetin demonstrated stability in binding to critical targets like MAPK14 and led to downregulation of phosphorylated p38 MAPK and JNK. *In vivo*, quercetin improved synovial tissue architecture and mitigated bone destruction. Mechanistic studies confirmed the dependency of effects of quercetin on the p38 MAPK pathway, supported by functional experiments using pathway agonists and inhibitors. The present study underscored the potential of quercetin in treating TMJ synovitis by modulating inflammatory signaling, promoting cell apoptosis and preserving bone integrity, thereby offering novel insights into therapeutic strategies for TMJ-related synovitis.

Correspondence to: Dr Yi Liu, School and Hospital of Stomatology, China Medical University, Liaoning Provincial Key Laboratory of Oral Disease, 117 Nanjing North Street, Heping, Shenyang, Liaoning 110002, P.R. China
E-mail: liuyiforstudent@163.com

Dr Xin Yi, Department of Oral Anatomy and Physiology, School and Hospital of Stomatology, China Medical University, Liaoning Provincial Key Laboratory of Oral Disease, 117 Nanjing North Street, Heping, Shenyang, Liaoning 110002, P.R. China
E-mail: yixinforstudent@163.com

*Contributed equally

Abbreviations: ANOVA, analysis of variance; BP, Biological Process; BV/TV, bone volume/tissue volume; CC, Cellular Component; CCK-8, Cell Counting Kit-8; cDNA, complementary DNA; CFA, Complete Freund's Adjuvant; ELISA, enzyme-linked immunosorbent assay; GO, Gene Ontology; H&E, hematoxylin and eosin; IHC, immunohistochemistry; KEGG, Kyoto Encyclopedia of Genes and Genomes; MCC, maximal clique centrality; MD, Molecular Dynamics; MF, Molecular Function; Micro-CT, micro-computed tomography; MM/PBSA, molecular mechanics/Poisson-Boltzmann surface area; MMP, matrix metalloproteinase; mean ± SD, mean ± standard deviation; NSAIDs, nonsteroidal anti-inflammatory drugs; OD, optical density; p-ERK, phosphorylated ERK; p-JNK, phosphorylated JNK; p-p38 MAPK, phosphorylated p38 MAPK; PPI, protein-protein interaction; qPCR, quantitative PCR; RA, rheumatoid arthritis; Rg, radius of gyration; RMSD, root-mean-square deviation; RMSF, root-mean-square fluctuation; ROI, region of interest; SD, Sprague-Dawley; Tb.N, trabecular number; Tb.Sp, trabecular separation; TMDs, temporomandibular disorders; TMJ, temporomandibular joint

Key words: quercetin, synovitis, temporomandibular disorders, p38 MAPK signaling pathway, inflammatory cytokines, bone destruction

Introduction

Temporomandibular disorders (TMDs) are a group of clinical conditions involving the temporomandibular joint (TMJ) and/or masticatory muscles, characterized by shared symptoms, including joint structural abnormalities, occlusal disturbances, muscular dysfunction and psychological factors (1). It is estimated that ~34% of the global population is affected by TMD each year (2,3). Although TMDs can exhibit a degree of self-limiting behavior, lack of timely and effective early intervention often leads to delayed recovery, progressive TMJ dysfunction, structural deformities and even craniofacial dysmorphisms, ultimately imposing long-term burdens on physical and psychological well-being of patients (4). Therefore, early intervention is critically important in halting the progression of TMD. The pathophysiology of TMD is complex, with inflammation playing a central role. Unlike the pronounced synovial inflammation observed in

rheumatoid arthritis (RA), TMD is typically considered a low-grade inflammatory state (5). Nevertheless, the inflammatory microenvironment of the synovium remains a key therapeutic target in TMD, as with RA. Current early-stage treatments for TMDs include physical therapy and occlusal splints, which require high patient compliance and frequent clinical visits, burdening individuals (6). Nonsteroidal anti-inflammatory drugs (NSAIDs) and corticosteroids can offer temporary pain relief during acute episodes but are unsuitable for long-term use due to adverse side effects (7). Commonly used chondroprotective agents, such as glucosamine, primarily target cartilage repair but lack efficacy in directly modulating synovitis over the long term (8,9). Thus, there is an urgent need to develop a safe, convenient and effective pharmacological strategy.

Quercetin (also known as Diosmetin) is a natural flavonoid compound predominantly found in citrus fruits, legumes and other plant-based sources (10). A growing body of recent reviews highlights its diverse pharmacological properties, including anti-inflammatory, anticancer and antioxidant activities (11-15). Emerging evidence suggests that quercetin may slow subchondral bone loss by inhibiting osteoclastogenesis, positioning it as a promising therapeutic agent for osteoarthritis (16). However, the effects of quercetin on the TMJ, particularly its pharmacological role and underlying mechanisms in TMJ synovitis, remain largely unexplored. In recent years, the advent of network pharmacology and molecular docking techniques has provided novel strategies for investigating the mechanisms of natural compounds (17,18). These technologies can systematically analyze drug targets and signaling pathways associated with diseases to reveal their potential therapeutic mechanisms.

Although the therapeutic efficacy of quercetin has been preliminarily validated in various inflammatory diseases (19), its specific role in TMD-related synovitis, particularly whether it exerts anti-inflammatory effects via the p38 MAPK signaling pathway, has not been systematically investigated. The p38 MAPK signaling pathway is known to play a critical role in regulating synovial inflammation and cell apoptosis and has been implicated in the pathogenesis of numerous inflammatory conditions (20-22). Exploring whether quercetin can modulate this pathway offers important theoretical value for understanding its mechanism of action. Although several treatments have shown efficacy in alleviating TMD symptoms, there remains a lack of pharmacological agents capable of providing long-term control of synovitis by targeting specific signaling pathways (23,24). Therefore, investigating whether quercetin can improve the clinical manifestations of TMD synovitis through a defined molecular mechanism, especially by modulating the p38 MAPK signaling pathway, holds innovative potential.

The present study aimed to investigate the potential therapeutic effects of quercetin in TMD-related synovitis, with a particular focus on verifying whether quercetin alleviates synovial inflammation by modulating the p38 MAPK signaling pathway, thereby promoting synoviocyte apoptosis and inhibiting subchondral bone destruction. From a scientific perspective, this research filled a critical knowledge gap regarding the role of quercetin in TMD synovitis and elucidated its underlying mechanism of action through the regulation of the p38 MAPK signaling pathway. The findings are expected to provide a theoretical foundation for the clinical application of quercetin in inflammatory joint disorders. Clinically, as a natural compound with proven safety and bioactivity, quercetin holds marked promise. If its efficacy is confirmed, the present study could offer a novel pharmacological strategy for treating TMD, particularly for early-stage, non-invasive, or adjunctive therapy. Ultimately, the outcomes of this research may contribute to improving patient quality of life, slowing disease progression and enhancing long-term prognosis in TMD while promoting the clinical translation of natural products in inflammatory disease management.

Materials and methods

Identification and intersection analysis of potential targets of quercetin in the treatment of TMJ synovitis. To identify potential therapeutic targets associated with TMJ synovitis, disease-related genes were retrieved using the keywords 'synovitis' and 'temporomandibular joint' from the DisGeNET (https://www.disgenet.org/), GeneCards (https://www.genecards.org/) and OMIM (https://omim.org/) databases. Meanwhile, the potential targets of quercetin were predicted using SwissTargetPrediction (http://www.swisstargetprediction.ch/), SuperPred (https://prediction.charite.de/) and PharmMapper (http://lilab-ecust.cn/pharmmapper), with the species restricted to *Homo sapiens*. An intersection analysis was performed between the disease-related targets and the quercetin-predicted targets. All candidate proteins were then standardized using the UniProt database (https://www.uniprot.org/) to obtain the official human gene names. The overlapping targets, representing potential key quercetin targets in TMJ synovitis, were identified and visualized using a Venn diagram generated by a bioinformatics visualization platform(http://www.bioinformatics.com.cn/).

Construction of the protein-protein interaction (PPI) network and identification of core targets. To further investigate the potential mechanisms by which quercetin exerts therapeutic effects on TMJ synovitis, 95 intersecting target genes were imported into the STRING database (https://cn.string-db.org/). The species was set to *Homo sapiens* and the minimum required interaction confidence score was set to 0.07 to construct a high-confidence PPI network. The PPI network data (in TSV format) were downloaded and imported into Cytoscape software (version 3.10.1; https://cytoscape.org/) for visualization and topological analysis. The NetworkAnalyzer plugin was used to calculate the topological parameters of each node, including degree centrality, betweenness centrality and closeness centrality, to comprehensively evaluate the importance of each protein within the network. Core target identification was performed using the CytoHubba plugin in Cytoscape. Nodes were ranked based on the Maximal Clique Centrality (MCC) algorithm (25) and the top 10 key targets were selected to construct a core subnet, which was then prioritized for subsequent mechanistic studies.

Gene Ontology (GO) and Kyoto Encyclopedia of Genes and Genomes (KEGG) signaling pathway enrichment analysis. Functional annotation and signaling pathway enrichment analysis were performed using the DAVID database (https://david.ncifcrf.gov/tools.jsp). GO enrichment analysis included three major categories: Biological Process (BP), Molecular Function (MF) and Cellular Component (CC). KEGG analysis was used to identify markedly enriched signaling pathways. All GO terms and pathways were ranked based on adjusted P-values and the false discovery rate (FDR) was applied to correct for multiple hypothesis testing and reduce false-positive results. The enrichment results were then imported into a bioinformatics visualization platform (http://www.bioinformatics.com.cn/) and displayed in the form of bar plots and bubble charts to intuitively present the most markedly enriched GO terms and KEGG pathways.

Molecular docking validation. The three-dimensional crystal structures of target proteins were obtained from the Protein Data Bank (PDB; https://www.rcsb.org/). PyMOL (v2.1; https://pymol.org/2/) removed impurities such as ligands, small molecular ions and water molecules. The preprocessed protein structures were imported into AutoDock Tools (v1.5.6; http://autodock.scripps.edu/resources/adt), where polar hydrogens were added, Gasteiger charges were assigned and atom types were specified. The prepared protein structures were saved in the .pdbqt format for subsequent docking analysis. The chemical structure of quercetin was retrieved from the PubChem database (https://pubchem.ncbi.nlm.nih.gov/). The molecular geometry was optimized using Chem3D (https://www.perkinelmer.com/category/chemdraw) through energy minimization and the structure was converted to .mol2 format. It was then imported into AutoDock Tools, where charges were added and rotatable bonds were defined. The final ligand structure was saved as a .pdbqt file. Docking grid boxes were defined based on the active site residues of the target proteins, with specified center coordinates and box dimensions. Molecular docking was performed using AutoDock Vina and the resulting binding conformations were ranked according to binding affinity (kcal/mol). The conformation with the lowest binding energy was selected as the optimal binding pose. The protein-ligand complexes were visualized using PyMOL to display the three-dimensional binding modes. Key interaction residues, such as hydrogen bonds and hydrophobic interactions, were analyzed to provide a structural basis for subsequent mechanistic investigations.

Molecular dynamics (MD) simulation. MD simulations were conducted on the protein-ligand complexes with the highest binding affinities obtained from docking analysis to further evaluate the binding stability and interaction characteristics between quercetin and its target proteins. The simulations were performed using the GROMACS software package (v.2020; https://www.gromacs.org/). The AMBER99SB-ILDN force field was applied for the protein components, while the General AMBER Force Field (GAFF) was used for the small-molecule ligand. Ligand topology files were generated using the sobtop tool and the atomic charges were calculated using the Restrained Electrostatic Potential method (26). The solvent environment was constructed using the TIP3P water model (27), with a solvation box extending at ≤1.0 nm from the protein atoms in all directions. Counterions (Na^+ or Cl^-) were added to neutralize the system based on the total charge. Following system construction, energy minimization was performed using the steepest descent algorithm to eliminate unfavorable contacts. The system was then subjected to an NVT ensemble (constant number of particles, volume and temperature) for 50 psec to gradually raise the temperature to 300 K for thermal equilibration. This was followed by a 50 psec NPT ensemble (constant number of particles, pressure and temperature) equilibration phase. A 100 nsec production MD simulation was subsequently carried out to assess the structural stability and dynamic interactions of the protein-ligand complexes under physiological conditions. The binding free energy ($\Delta G_{binding}$) between the protein and ligand was calculated using the molecular mechanics/Poisson-Boltzmann surface area (MM/PBSA) method with the g_mmpbsa tool in GROMACS (https://g_mmpbsa.readthedocs.io/), providing a quantitative evaluation of complex stability.

Cell culture and treatment. The human synovial cell line SW982 was obtained from the National Certified Cell Bank and cultured in L-15 medium (Gibco; Thermo Fisher Scientific, Inc.; cat. no. 11415064) supplemented with 10% fetal bovine serum (FBS, Gibco; Thermo Fisher Scientific, Inc.; cat. no. A5669401) and 1% penicillin-streptomycin solution (Gibco; Thermo Fisher Scientific, Inc.; cat. no. 15140122). Cells were maintained at 37˚C in a humidified incubator with 5% CO_2. To establish an *in vitro* inflammatory model, cells were stimulated with 10 ng/ml recombinant human IL-1β (PeproTech, Inc.) for 24 h. Following stimulation, cells were treated with quercetin (MedChemExpress; cat. no. HY-N0125,) at concentrations of 20, 40 and 80 μM for an additional 24 h. Quercetin was dissolved in DMSO and diluted to the desired concentrations, ensuring the final DMSO concentration did not exceed 0.1%. The experimental groups included i) untreated control, ii) IL-1β-only model group and iii) IL-1β + quercetin treatment groups at different concentrations. All experiments were performed in biological replicates to ensure data reliability.

To investigate pathway-specific mechanisms, p38 MAPK signaling pathway modulators were applied. After 24 h of IL-1β (10 ng/ml) stimulation, SW982 cells were pretreated for 30 min with either the p38 MAPK activator anisomycin (10 μM; MedChemExpress; cat. no. HY-18982) or the inhibitor SB203580 (10 μM, HY-10256, MedChemExpress), followed by co-treatment with 40 μM quercetin for another 24 h (28,29). Subsequent assays included cell viability analysis Cell Counting Kit-8 (CCK-8), apoptosis detection (Annexin V/PI flow cytometry), inflammatory cytokine quantification enzyme-linked immunosorbent assay (ELISA) and protein expression analysis of phosphorylated p38 MAPK (p-p38 MAPK; western blotting). The experimental setup consisted of five groups: i) Control; ii) IL-1β; iii) IL-1β + quercetin; iv) IL-1β + quercetin + SB203580 all v) IL-1β + quercetin + anisomycin. All experiments were conducted in triplicate to ensure reproducibility.

Cell proliferation assay. SW982 cells were seeded into 96-well plates at a density of $1x10^4$ cells per well and allowed to adhere for 24 h. After attachment, the cells were treated with IL-1β (10 ng/ml) combined with various concentrations of quercetin (2.5, 5, 10, 20, 40, 80 and 100 μM) and incubated for 24 h. Following treatment, 10 μl of CCK-8 reagent (Saint-Bio; cat. no. ST1008) was added to each well and incubated at 37˚C for 2 h. The optical density (OD) at 450 nm was measured using a microplate reader (Multiscan MK3, Thermo Fisher Scientific, USA) to assess cell viability.

Apoptosis assay. SW982 cells were seeded in 6-well plates and treated with quercetin at 20, 40 and 80 μM concentrations for 48 h. Following treatment, cells from each group were harvested and washed twice with PBS. Apoptosis was assessed using an Annexin V-APC/7-AAD dual-staining apoptosis detection kit (Nanjing KeyGen Biotech Co., Ltd.; cat. no. KGA1106). Then, ~$1x10^6$ cells per group were resuspended in 500 μl of binding buffer, followed by the addition of 5 μl Annexin V-APC and 5 μl 7-AAD. The samples were incubated in the dark at room temperature for 15 min. Stained cells were then analyzed using a flow cytometer (FACSCalibur, BD Biosciences), with at least 10,000 events collected per sample. Flow cytometric data were analyzed using FlowJo software (version 10.0; BD Biosciences). Cell debris was excluded by forward scatter and side scatter gating and apoptotic cells were identified based on staining patterns: Early apoptosis (Annexin V^+/7-AAD^-) and late apoptosis (Annexin V^+/7-AAD^+). The apoptosis rate for each treatment group was subsequently calculated. The total apoptosis rate was calculated as the sum of the percentages of early (Annexin V^+/7-AAD^-) and late (Annexin V^+/7-AAD^+) apoptotic cells.

ELISA. After 24 h of treatment, the culture supernatants of SW982 cells were collected and centrifuged at 1,000 x g for 10 min to remove cellular debris. The clarified supernatants were reserved for subsequent analysis. The protein levels of matrix metalloproteinase 3 (MMP3), MMP9 and MMP13 were measured using ELISA kits (Wuhan Boster Biological Technology, Ltd.; cat. nos. EK0461, EK0465 and EK0486), following the manufacturer's instructions. All samples were assayed in duplicate and standard curves were generated to convert OD values into concentrations (pg/ml). OD values were measured at 450 nm using a microplate reader (Infinite F200; Tecan Group, Ltd.), with background subtraction based on blank wells. The resulting data were used to evaluate differences in the expression levels of inflammatory cytokines among the various treatment groups.

Western blot analysis. Western blotting was performed to detect the expression levels of inflammation-related signaling pathway proteins in SW982 cells. Total protein was extracted using RIPA lysis buffer (Beyotime Institute of Biotechnology; cat. no. P0013B), and protein concentrations were determined using a BCA protein assay kit (Beyotime Institute of Biotechnology). Equal amounts of protein (20 μg per lane) were separated by 10% SDS-PAGE and transferred onto PVDF membranes (MilliporeSigma; cat. no. IPVH00010). Membranes were blocked with 5% BSA (MilliporeSigma) at room temperature for 1 h. Subsequently, the membranes were incubated overnight at 4˚C with the following primary antibodies: p-p38 MAPK (Thr180/Tyr182; cat. no. 9211) and total p38 MAPK (cat. no. 9212) from Cell Signaling Technology, Inc.; phosphorylated (p-)JNK, JNK, p-ERK, and ERK (cat. nos. SC7345, SC6254, SC7348, and SC514302) from Santa Cruz Biotechnology, Inc.; IL-6, TNF-α, and β-Tubulin (cat. nos. ab315214, ab9324, and ab307164) from Abcam. After washing, membranes were incubated for 1 h with HRP-conjugated goat anti-rabbit or anti-mouse secondary antibodies (cat. nos. ab205718 and ab205719, Abcam). Protein bands were visualized using an ECL detection reagent (Tanon Science and Technology Co., Ltd.) and imaged with the Tanon 4600 chemiluminescence imaging system (Tanon Science and Technology Co., Ltd.). Band intensities were quantified using ImageJ software (NIH, version 1.8.0), and β-Tubulin was used as the internal loading control.

Animal experiments. A total of 20 male Sprague-Dawley (SD) rats (7-8 weeks old; weighing 200-250 g) were obtained from an accredited laboratory animal center. Specifically, all animals were purchased from Beijing Vital River Laboratory Animal Technology Co., Ltd. (Beijing, China), and housed under standard conditions (22±2˚C, 50±10% humidity, and a 12-h light/dark cycle) with free access to food and water. All experimental procedures were approved by the Animal Ethics Committee of China Medical University (approval no: kt2022112) and conducted by institutional guidelines (30). The TMJ synovitis model was established based on a previously described method (31), with slight modifications. Inflammation was induced by intra-articular injection of 50 μl of complete Freund's adjuvant (CFA) into both TMJ cavities. One week after model induction, drug administration was initiated and continued daily for 14 consecutive days. Quercetin was dissolved in propylene glycol and administered orally via gavage once daily. The animals were randomly divided into four groups (n=5 per group): Control group: Bilateral injection of 50 μl saline; CFA group: Bilateral injection of 50 μl CFA; CFA + 20D group: CFA injection followed by quercetin treatment at 20 mg/kg/day; CFA + 40D group: CFA injection followed by quercetin treatment at 40 mg/kg/day.

Tissue collection and processing. At the end of the treatment period (Day 28), rats were euthanized by intraperitoneal injection of an overdose of sodium pentobarbital. Bilateral TMJ were collected for subsequent analyses and allocated to the following experimental procedures:

Micro-computed tomography (Micro-CT): TMJ tissues were fixed in 4% paraformaldehyde for 24 h at 4˚C, and then transferred to 70% ethanol for storage before scanning and morphometric analysis.

Histological Staining: Samples were decalcified in 10% EDTA solution at room temperature for 4 weeks, followed by paraffin embedding and sectioning.

ELISA: Synovial tissues were isolated and immediately stored at -80˚C.

Reverse transcription-quantitative (RT-q) PCR. Total RNA was extracted from SW982 cells and rat synovial tissues. SW982 cells were seeded at a density of $1x10^6$ cells per

well in 6-well plates prior to RNA extraction. Samples were lysed using TRIzol® reagent (Invitrogen; Thermo Fisher Scientific, Inc.; cat. no. 15596026), and RNA was purified using the MiniBEST Universal RNA Extraction Kit (Takara Biotechnology Co., Ltd.; cat. no. 9767), following the manufacturer's protocol. RNA purity and concentration were assessed using a NanoDrop 2000 spectrophotometer (Thermo Fisher Scientific, Inc.), and samples with A260/A280 ratios between 1.8 and 2.0 were used for further experiments.

For each sample, 1 μg of total RNA was reverse-transcribed into complementary DNA (cDNA) using PrimeScript™ RT Master Mix (Takara Biotechnology Co., Ltd.; cat. no. RR036A), according to the manufacturer's instructions. qPCR was carried out using the SYBR® Premix Ex Taq II (Takara Biotechnology Co., Ltd.; cat. no. RR820A) in a 25 μl reaction mixture containing 10 μl SYBR Green mix, 1 μl forward primer, 1 μl reverse primer, 2 μl template cDNA, and 6 μl RNase-free water. The amplification program was as follows: initial denaturation at 95˚C for 30 sec, followed by 40 cycles of denaturation at 95˚C for 5 sec and annealing/extension at 60˚C for 34 sec. All reactions were performed in triplicate and each experiment was independently repeated three times.

Relative gene expression levels were calculated using the $2^{-\Delta\Delta Cq}$ method as described by Livak and Schmittgen (32). GAPDH was used as the internal reference gene depending on species. The sequences of all primers used for qPCR are listed in Tables SI (human) and SII (rat).

ELISA detection. To evaluate the expression levels of inflammation-related cytokines and proteins involved in the MAPK signaling pathway, ELISA assays were performed on both the culture supernatants of SW982 cells and total protein extracts from rat synovial tissues.

After treatment with various concentrations of quercetin for 24 h, culture supernatants from SW982 cells were collected and centrifuged at 1,000 x g for 10 min at 4˚C to remove cellular debris. MMP3, MMP9 and MMP13 concentrations were measured using commercial ELISA kits Wuhan Boster Biological Technology, Ltd.; cat. nos. EK0461, EK0465 and EK0486), following the manufacturer's protocols. All samples were analyzed in technical duplicates (n=2) and protein concentrations (pg/ml) were calculated based on standard curves. Absorbance was measured at 450 nm using a microplate reader (Infinite F200; Tecan Group, Ltd.), with background correction applied. The results were used to analyze changes in MMP secretion among the different treatment groups.

For synovial tissue, total protein was extracted and analyzed using the InstantOne ELISA kits (Thermo Fisher Scientific, Inc.; cat. no. 85-86195) to detect the phosphorylation levels of p-ERK1/2, p-p38 MAPK and p-JNK. Equal amounts of protein were added to each well, followed by 50 μl of antibody working solution per well. The plates were incubated at room temperature for 1 h in the dark. After incubation, the plates were washed three times and substrate solution was added. The reaction was terminated and absorbance was measured at 450 nm. The resulting data were used to compare the activation levels of MAPK signaling pathway components between groups.

Histological staining. Following decalcification, condylar tissues were dehydrated using a graded ethanol series and embedded in paraffin. Serial midsagittal sections with a thickness of 4 μm were prepared. Hematoxylin and eosin (H&E) staining was performed at room temperature (22-25˚C), with hematoxylin staining for 8 min and eosin staining for 2 min, to assess the degree of synovitis. The synovial tissue sections were scored using the Gynther synovitis grading method (33).

Safranin O-Fast Green staining was conducted at room temperature (22-25˚C), with Fast Green staining for 3 min followed by Safranin O staining for 5 min, to evaluate the condylar cartilage structure and proteoglycan content. The stained sections were observed under a light microscope (Nikon Corporation). Cartilage matrix staining intensity and structural integrity were assessed using a previously established scoring system (34).

Immunohistochemistry (IHC) staining. IHC was performed to detect the expression of inflammation- and signaling pathway-related proteins in synovial tissue, including MMP13, IL-6 and p-p38 MAPK. Paraffin-embedded tissue sections were deparaffinized, rehydrated and incubated overnight at 4˚C with the following primary antibodies: MMP13 (Abcam; cat. no. ab237604; 1:2,000), IL-6 (Abcam; cat. no. ab9324; 1:500) and p-p38 MAPK (Cell Signaling Technology, Inc.; cat. no. 4511, 1:400). The following day, color development was performed using a DAB chromogenic substrate. Sections without primary antibodies served as negative controls. After staining, the relative protein expression levels in the synovial tissue were quantified using Image Pro Plus software (version 6.0.0.260; Media Cybernetics) by measuring the integrated optical density (IOD) across multiple fields of view.

Dual immunofluorescence staining and co-localization analysis. Paraffin-embedded synovial tissue sections (4 μm thick) were deparaffinized, rehydrated and subjected to high-temperature antigen retrieval in 0.01 M citrate buffer (pH 6.0). After cooling to room temperature, sections were permeabilized with 0.3% Triton X-100 for 10 min. All washing steps were performed using PBS (pH 7.4). Non-specific binding sites were blocked using 5% goat serum (Beyotime Institute of Biotechnology) at room temperature for 1 h. Sections were then incubated overnight at 4˚C in the dark with the following combinations of primary antibodies: p-p38 MAPK (Cell Signaling Technology, Inc.; cat. no. 4511, 1:400) + IL-6 (Abcam; cat. no. ab9324; 1:500), or p-p38 MAPK + MMP13 (Abcam; cat. no. ab237604; 1:500). The next day, Alexa Fluor® 488-conjugated goat anti-mouse IgG (Thermo Fisher Scientific, Inc.; cat. no. A11008) and Alexa Fluor® 594-conjugated goat anti-rabbit IgG (cat. no. A11012) secondary antibodies were applied at a dilution of 1:500 for 1 h at room temperature in the dark. Nuclei were counterstained with DAPI (Thermo Fisher Scientific) at room temperature for 5 min. After mounting, images were acquired using a confocal laser scanning microscope (Nikon A1; Nikon Corporation) at 400x magnification under consistent exposure settings. Co-localization and fluorescence intensity analysis were performed using ImageJ software (NIH, version 1.8.0). The fluorescence intensity of overlapping regions in the red and green channels was quantified and expressed as relative

fluorescence intensity (Relative fluorescence intensity, A.U.) for subsequent statistical comparisons.

Micro-CT and 3D reconstruction. To evaluate the protective effect of quercetin on condylar bone structure, bilateral TMJ samples were collected from rats and subjected to bone morphometric analysis using a Micro-CT system. The scanning parameters were set as follows: 80 kV voltage and 56 μA current. The acquired raw data were processed and reconstructed in three dimensions using CTAn and CTVox software (Bruker Corporation). A cylindrical region of interest (ROI) with a diameter of 0.86 mm and a height of 0.765 mm was selected beneath the interface between the anterior condylar cartilage and the subchondral bone. This ROI was used for quantitative analysis of trabecular bone microarchitecture. The analyzed parameters included Bone Volume/Tissue Volume (BV/TV): the ratio of bone volume to total tissue volume; Trabecular Thickness (Tb.Th); Trabecular Number (Tb.N); Trabecular Separation (Tb.Sp). All parameters were automatically calculated according to the standard protocols of the Micro-CT system. The results were used to compare changes in trabecular bone structure among the different treatment groups.

Statistical analysis. All experimental data were presented as the mean ± standard deviation (mean ± SD). Prior to intergroup comparisons, data were tested for normality using the Shapiro-Wilk test and for homogeneity of variance using Levene's test to ensure the assumptions for parametric analysis were met. For comparisons between two independent groups, two-tailed independent sample t-tests were conducted. For comparisons among multiple groups, one-way analysis of variance (ANOVA) was performed, followed by post hoc multiple comparisons using Tukey's HSD or Bonferroni correction to control for false-positive results. Statistical analyses and graphical plotting were conducted using GraphPad Prism 6.0 software (Dotmatics). $P<0.05$ was considered to indicate a statistically significant difference. Significance levels were indicated as: $^{*}P<0.05$, $^{**}P<0.01$ and $^{***}P<0.001$.

Results

Bioinformatics reveals that quercetin may alleviate TMJ synovitis by targeting core genes in the MAPK signaling pathway. To systematically explore the potential mechanisms by which quercetin alleviates TMJ synovitis, a network pharmacology-based approach was employed to integrate data from multiple databases (Fig. 1A). The 2D chemical structure of quercetin was retrieved from the PubChem database (Fig. 1B). 435 potential quercetin targets were predicted using SwissTargetPrediction, SuperPred and PharmMapper Server. Meanwhile, 993 synovitis-related targets and 165 TMJ disorder-related targets were collected from GeneCards, OMIM and DisGeNET databases. An intersection analysis identified 95 overlapping genes potentially involved in disease modulation (Fig. 1C). To further investigate the underlying mechanism, these 95 intersecting targets were imported into the STRING database to construct a PPI network, which was then visualized using Cytoscape software (v3.10.1; Fig. 1D). After removing disconnected nodes, the reconstructed network included 83 nodes and 321 edges, indicating high interconnectivity among targets. The network exhibited a median degree centrality of 15.47 and a betweenness centrality of 141.59, suggesting that several nodes exert strong regulatory influence. Using the CytoHubba plugin and the MCC algorithm, the top 10 hub genes were identified, including MAPK14, MMP13 and IL6 (Fig. 1E). These genes displayed high connectivity within the PPI network and were markedly enriched in GO and KEGG pathway analyses, indicating their potential role as key targets through which quercetin exerts its anti-inflammatory effects.

GO and KEGG enrichment analyses reveal that quercetin targets may alleviate synovitis via regulation of the IL-17 and MAPK signaling pathways. GO and KEGG enrichment analyses were conducted on the 95 intersecting candidate targets to gain deeper insights into the functional characteristics of potential of quercetin targets. GO enrichment covered three major categories: BP, MF and CC (Fig. 2A). In the BP category, the target genes were markedly enriched in terms such as 'positive regulation of cell migration', 'activation of phosphatidylinositol 3-kinase signaling', and 'proteolysis'. For MF, significant enrichments included 'serine-type endopeptidase activity', 'tyrosine kinase activity', and 'enzyme binding'. In the CC category, the targets were predominantly localized to the 'extracellular region,' 'membrane structure', and 'exosomes'.

KEGG pathway enrichment analysis further identified several highly significant inflammation-related signaling pathways, including the IL-17 signaling pathway, MAPK signaling pathway, TNF signaling pathway and PI3K-Akt signaling pathway (Fig. 2B). Integrating these findings with the PPI network topology analysis, key hub targets such as MAPK14, MMP13 and IL6 were primarily enriched in the IL-17 and MAPK pathways. These results suggest that quercetin may exert its therapeutic effects on TMJ synovitis by regulating these critical inflammatory signaling pathways.

Molecular docking confirms stable binding of quercetin to key targets in the IL-17 and MAPK signaling pathways. To further validate the biological relevance of the GO and KEGG enrichment results, molecular docking analyses were performed using key proteins enriched in the IL-17 and MAPK signaling pathways, aiming to assess the structural binding affinity of quercetin to these core targets. A total of 23 representative proteins were selected as docking candidates, including GSK3B, MMP13, MMP1, CASP3, MMP3, PTGS2, MMP9, S100A9, MAPK1, MAPK8, MAPK14, NFKB1, PDGFRB, FLT3, IGF1, EGFR, KIT, KDR, AKT1, TEK, PTPN7, HARS and FGFR1. These targets encompass protein kinases, transcription factors and inflammatory effectors. Molecular docking was performed using AutoDock Vina and quercetin demonstrated favorable binding affinities across multiple targets, with binding energies below -7 kcal/mol. The strongest binding affinities were observed with MMP3, MMP9, MMP13, MAPK1, MAPK8 and MAPK14 (Table I), suggesting that these proteins may serve as direct binding targets of quercetin. Further structural analysis using PyMOL revealed key interactions between quercetin and these proteins, including hydrogen bonds and hydrophobic interactions, confirming the specificity

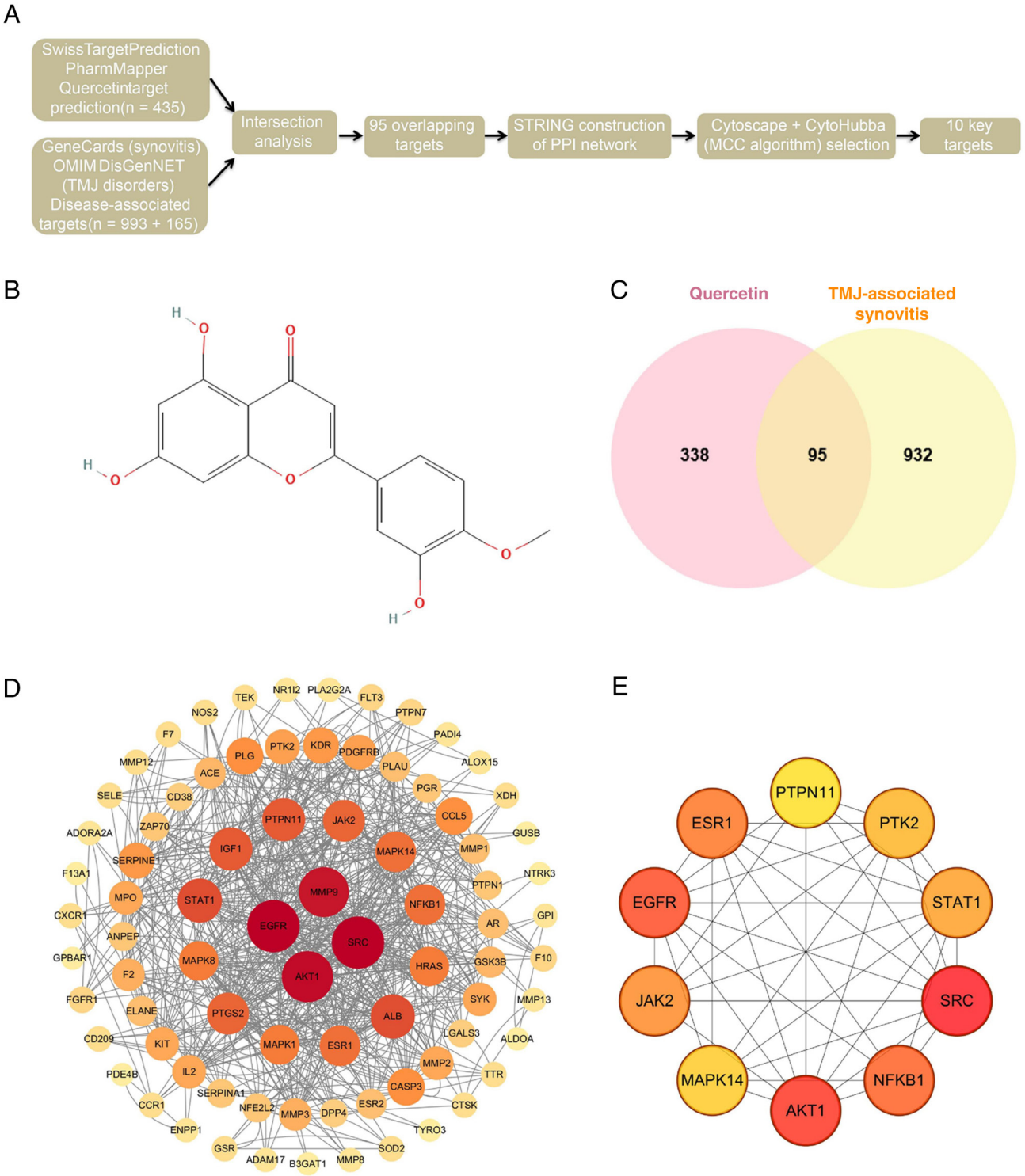

Figure 1. Network pharmacology analysis reveals key signaling pathways and core target genes of quercetin in synovitis. (A) Schematic workflow of network pharmacology analysis for identifying core targets; (B) 2D chemical structure of quercetin; (C) A total of 95 potential therapeutic targets were identified by intersecting quercetin-predicted targets with synovitis and TMJ disorder-related disease targets; (D) PPI network of the 95 targets constructed using the STRING database. Node size and color represent the degree of connectivity; (E) Top 10 hub genes identified by the MCC algorithm, including MAPK14, MMP13 and IL6. TMJ, temporomandibular joint; PPI, protein-protein interaction; MCC, maximal clique centrality; MMP, matrix metalloproteinase.

and stability of the binding conformations (Fig. 3A-F). These findings provide structural evidence supporting the hypothesis that quercetin mitigates inflammation by inhibiting MMP activity and MAPK phosphorylation, thereby laying a theoretical foundation for subsequent *in vitro* and *in vivo* validation experiments.

MD simulations confirm stable binding of quercetin to MAPK and MMP targets. To further validate the molecular docking results and assess the dynamic stability of quercetin-target interactions, 100-nsec MD simulations were performed on the six protein-ligand complexes with the lowest binding energies. The selected proteins, MMP3, MMP9, MMP13,

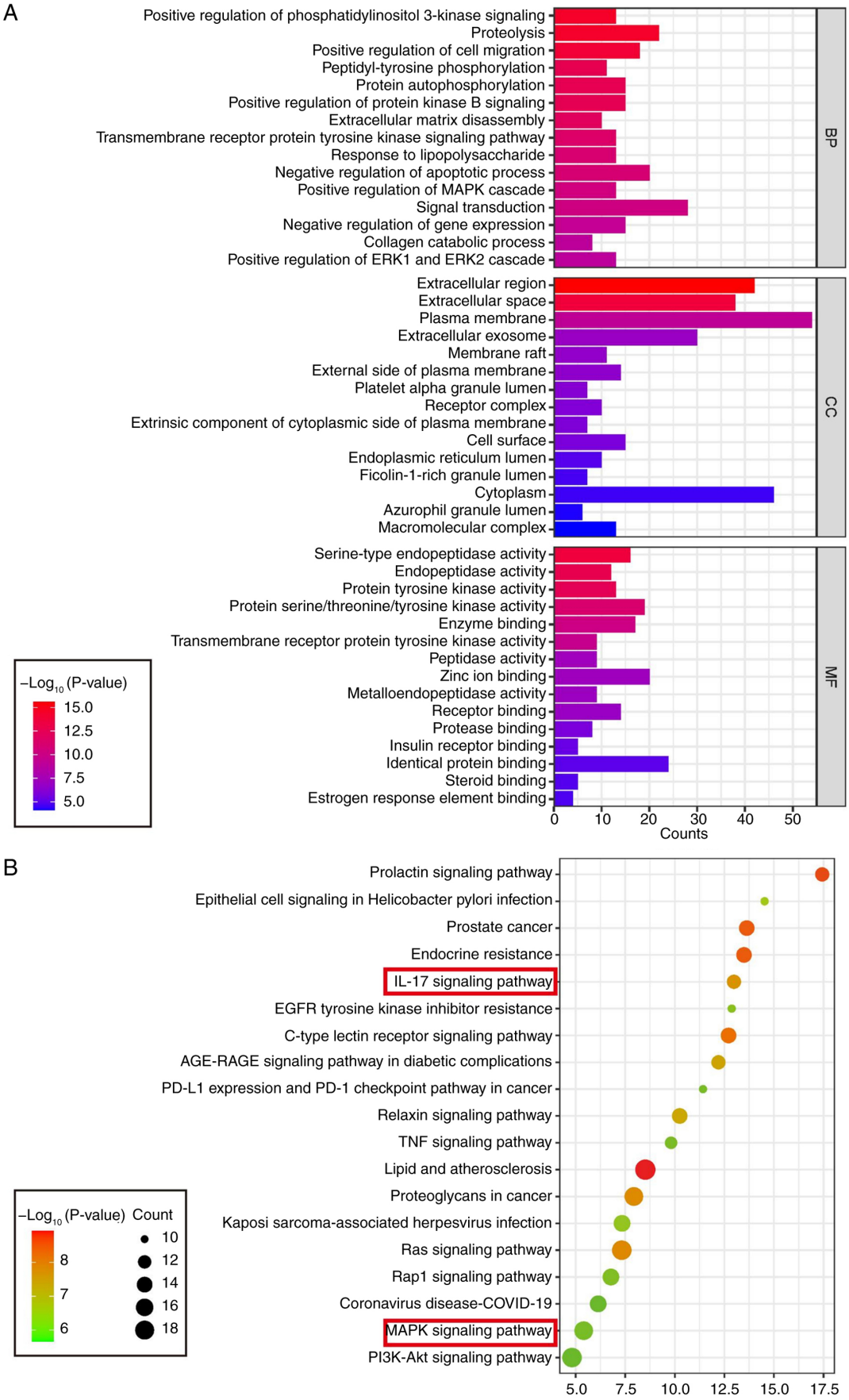

Figure 2. Identifying key signaling pathways and MF enrichment patterns associated with quercetin in synovitis. (A) GO enrichment analysis of potential of quercetin targets, showing the top 15 markedly enriched terms across three categories: BP, MF and CC; (B) KEGG pathway enrichment analysis of the predicted targets, displaying the top 15 markedly enriched signaling pathways. Notably, the IL-17, MAPK, TNF and PI3K-Akt pathways were among the most markedly enriched, suggesting that quercetin may exert anti-synovitis effects by modulating these inflammation-related pathways. GO, Gene Ontology; BP, Biological Process; MF, Molecular Function; CC, Cellular Component; KEGG, Kyoto Encyclopedia of Genes and Genomes.

Table I. The docking results for protein with diosmetin.

Target	Compound	Docking score (kcal/mol)
MMP3	Diosmetin	-6.45
MMP9	Diosmetin	-7.12
MMP13	Diosmetin	-7.12
MAPK1	Diosmetin	-7.30
MAPK8	Diosmetin	-7.30
MAPK14	Diosmetin	-8.30

MMP, matrix metalloproteinase.

MAPK1, MAPK8 and MAPK14, are core targets within the IL-17 and MAPK signaling pathways. Root-mean-square deviation (RMSD) analysis was used to evaluate the overall structural stability of the complexes. The RMSD values for all complexes remained within a reasonable range, indicating that the protein-ligand conformations were dynamically stable throughout the simulation period. Notably, the MMP9-quercetin complex exhibited an average RMSD of <2 Å and reached dynamic equilibrium ~25 nsec, reflecting excellent protein stability (Fig. 4A). Similarly, the MMP3-quercetin and MMP13-quercetin complexes maintained average RMSD values below 3 Å and 3.5 Å, respectively and reached relatively stable states after 20 nsec (Fig. 4A). For the MAPK complexes, the average RMSD values of MAPK1, MAPK8 and MAPK14 were below 2.5 Å, with stable conformations achieved after ~40 nsec (Fig. 4B). The RMSD analysis reflects the average deviation of the protein structures from their initial conformations over time, serving as a quantitative measure of system stability.

To assess the flexibility of amino acid residues during binding, root-mean-square fluctuation (RMSF) analysis was performed. The results revealed that most residues exhibited only minor fluctuations, with slight variations mainly localized to hinge regions or protein surface loops. All six protein-ligand complexes maintained structurally stable conformations throughout the simulation, indicating that quercetin binding did not induce significant conformational disruptions (Fig. 4C and D). The number of hydrogen bonds formed between quercetin and each target protein was monitored to further evaluate the interaction dynamics during the simulation. The number of hydrogen bonds remained relatively stable across the simulation period, ranging from 0-5 per complex (Fig. 4E and F). These hydrogen bonds served as key non-covalent forces contributing to the structural stability of the complexes.

The radius of gyration (Rg) was analyzed to measure each protein's compactness. Results showed that all proteins remained tightly folded throughout the 100 nsec simulation, with MMP9 and MAPK1 displaying the least fluctuation in Rg values, further supporting their classification as highly stable binding targets. Specifically, the Rg values of MMP9 and MMP13 fluctuated within the 1.51-1.62 nm range, while MAPK8 and MAPK14 ranged between 2.14 and 2.28 nm (Fig. 4G and H).

Binding free energies were calculated using the MM/PBSA method. As shown in Table II, all six protein-ligand complexes exhibited negative binding energies, indicating favorable thermodynamic stability. The binding affinity was primarily driven by van der Waals interactions and electrostatic forces, while solvent-accessible surface area (SASA) and polar solvation energy made smaller contributions.

In summary, MD simulations verified that quercetin can form stable complexes with multiple targets (particularly MAPK and MMP family members), providing the structural and energetic foundation for subsequent *in vitro* cellular experiments and animal studies to validate its anti-inflammatory mechanisms.

Quercetin reverses inflammatory-induced synoviocyte dysfunction by promoting apoptosis and inhibiting proliferation. Previous molecular docking and dynamics simulations suggested that quercetin can stably bind to key targets such as MMPsec and MAPKs, indicating its potential to modulate signaling pathways associated with inflammation and cell proliferation. To further verify its biological effects at the cellular level, the present study investigated the regulatory role of quercetin in an *in vitro* inflammatory model of synoviocytes (Fig. 5A). An inflammatory state was established in SW982 cells by IL-1β (10 ng/ml) stimulation, followed by treatment with various concentrations of quercetin (0-100 μM). CCK-8 assay results showed that quercetin markedly inhibited IL-1β-induced abnormal proliferation in a dose-dependent manner within the range of 20-100 μM (Fig. 5B). Based on these findings, 20, 40 and 80 μM were selected for subsequent experiments. Flow cytometry analysis further demonstrated that quercetin treatment markedly increased the apoptosis rate of synoviocytes, showing a clear dose-dependent trend (Fig. 5C and 5D).

These results indicate that quercetin exhibits strong molecular binding to inflammation, and proliferation-related targets. It effectively suppresses inflammatory-induced synoviocyte overproliferation and promotes apoptosis at the cellular level. These findings provide a solid foundation for subsequent functional validation of its effects on MMP secretion and MAPK signaling pathway activity.

Quercetin attenuates synovial inflammation by regulating MMP expression and inhibiting MAPK signaling pathway phosphorylation. To further elucidate the anti-inflammatory mechanism of quercetin *in vitro*, its regulatory effects on MMPsec and inflammatory cytokines were examined. ELISA results showed that quercetin markedly reduced the secretion levels of MMP3, MMP9 and MMP13 under IL-1β stimulation, suggesting its potential role in protecting cartilage by inhibiting extracellular matrix degradation in synoviocytes (Fig. 6A). Additionally, western blot analysis revealed a dose-dependent decrease in the protein expression of inflammatory cytokines TNF-α, IL-1β and IL-6 following quercetin treatment (Fig. 6B), further supporting its anti-inflammatory effects. To determine whether these effects are mediated via the MAPK signaling pathway, the phosphorylation levels of key MAPK family members p38, ERK1/2 and JNK were assessed. The results demonstrated that quercetin markedly inhibited the phosphorylation of p38 MAPK and JNK, while

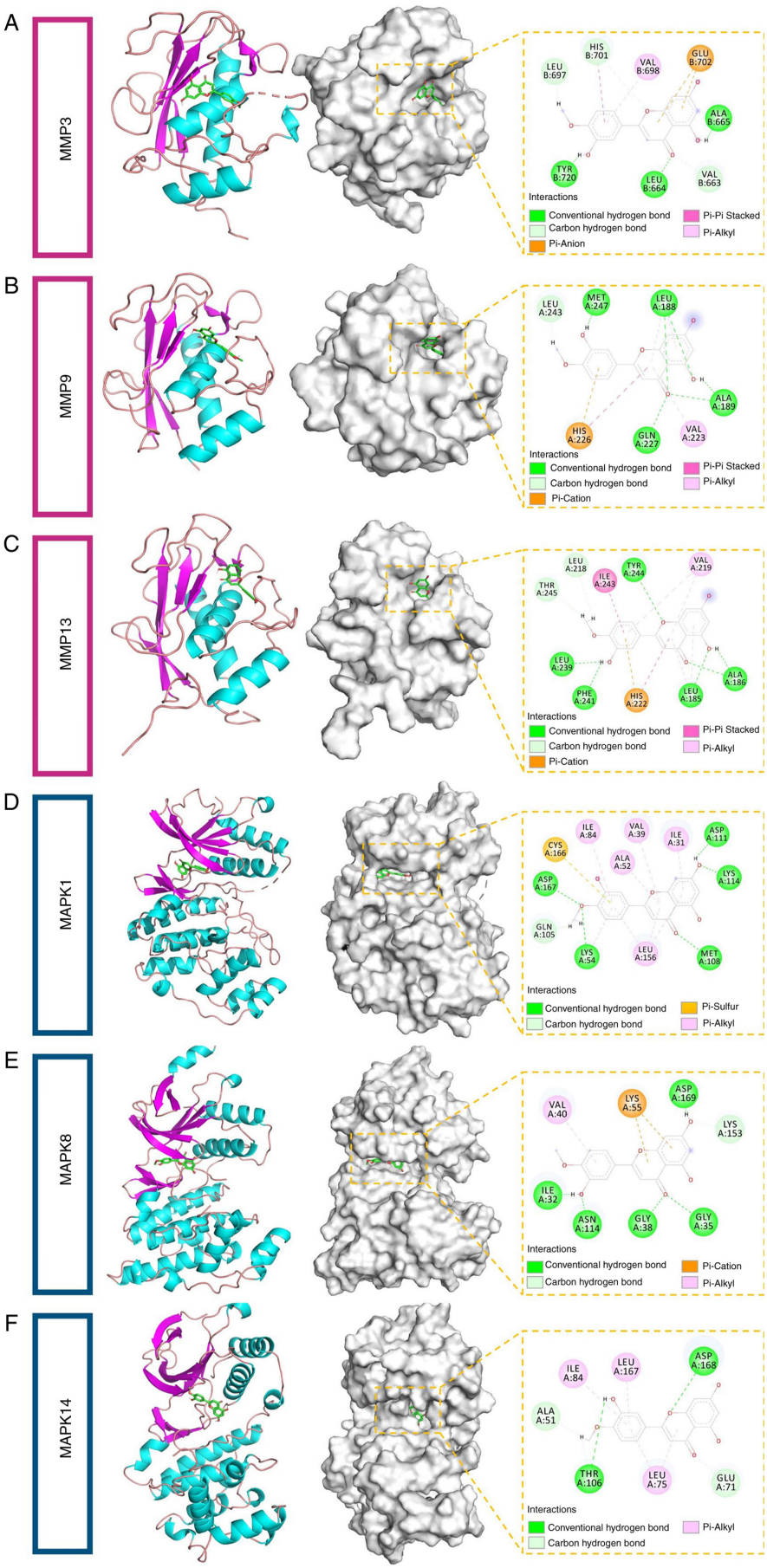

Figure 3. Molecular docking validation of quercetin binding to key targets in the MAPK and IL-17 signaling pathways. Binding modes of quercetin with (A) MMP3, (B) MMP9, (C) MMP13, (D) MAPK1, (E) MAPK8 and (F) MAPK14. Each panel illustrates the complex's three-dimensional structure, the protein's electrostatic surface and the two-dimensional interaction map of the protein-ligand complex.

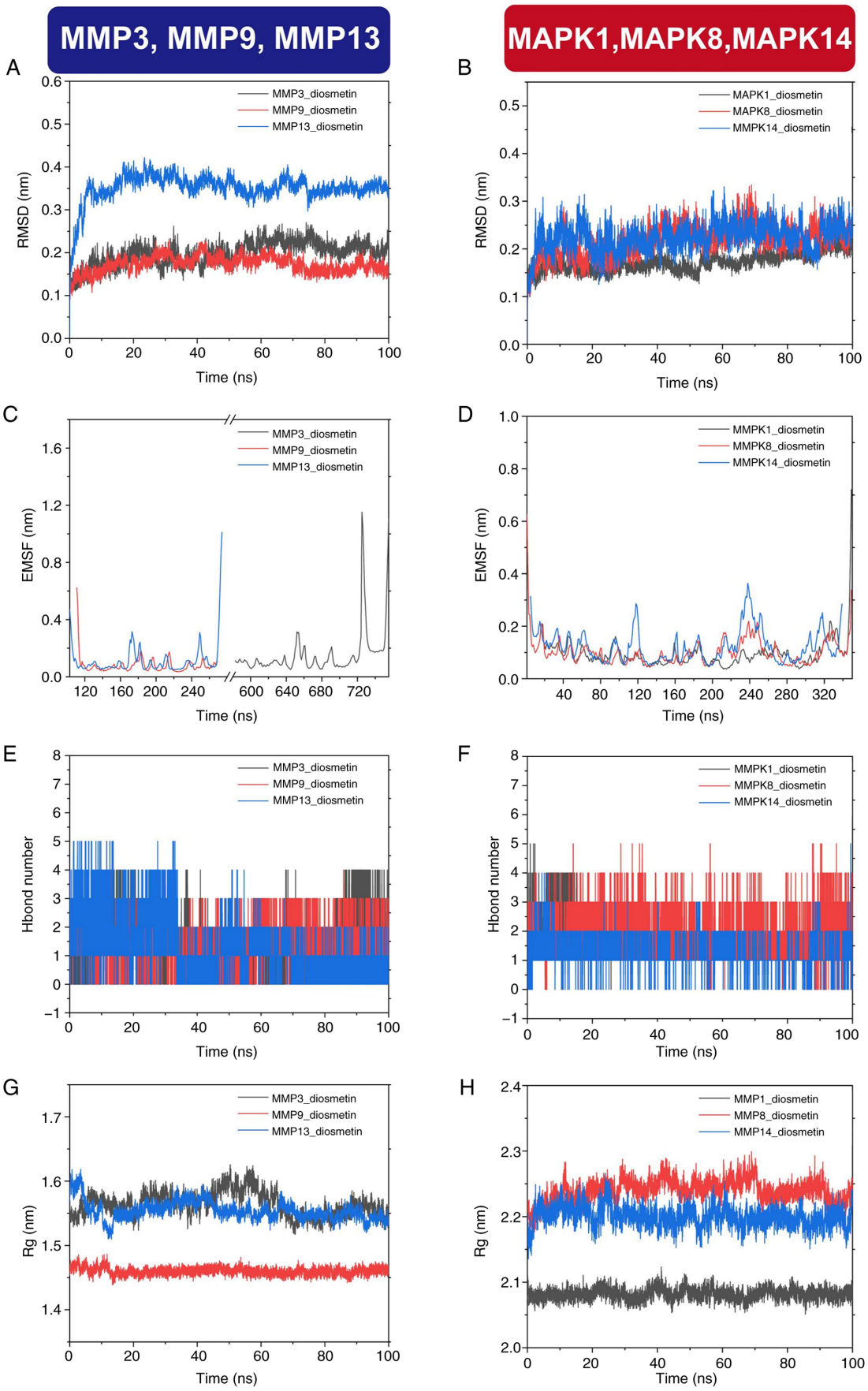

Figure 4. MD simulations evaluate the binding stability of quercetin with key target proteins. (A and B) The RMSD changes of each complex within 100 ns were evaluated to assess their overall structural stability; (C and D) RMSF analysis showing flexibility variations of individual protein residues; (E and F) Time-dependent changes in the number of hydrogen bonds, reflecting the physical stability of ligand binding; (G and H) Rg analysis assessing the compactness of protein structures. The results demonstrate that quercetin forms stable complexes with MMP and MAPK family targets. MD, Molecular Dynamics; RMSD, root-mean-square deviation; RMSF, root-mean-square fluctuation; Rg, radius of gyration; MMP, matrix metalloproteinase.

Table II. The binding energy by MMGBSA (KJ/mol).

Systems	EVDW	EELE	EGB	ESA	Gbinding energy
MMP3-Diosmetin	-108.058±11.266	-52.647±9.564	12.887±11.881	-3.174±0.658	-150.992±15.419
MMP9-Diosmetin	-94.776±15.567	-41.137±11.778	17.653±9.008	-3.084±0.184	-121.344±5.838
MMP13-Diosmetin	-28.588±6.169	-28.588±6.169	19.406±5.331	-121.344±5.838	-130.609±14.595
MAPK1-Diosmetin	-127.628±16.138	-67.43±9.475	132.512±18.163	-14.56±0.618	-77.106±12.674
MAPK8-Diosmetin	-138.591±8.773	-53.998±16.495	142.141±15.198	-15.028±0.662	-65.475±9.43
MAPK14-Diosmetin	-136.477±13.193	-46.145±12.439	141.91±18.201	-16.068±0.773	-56.78±12.6

MMGBSA, molecular mechanics generalized born surface area; MMP, matrix metalloproteinase; EVDW, van der Waals energy; EELE, electrostatic energy; EGB, polar contribution to solvation; ESA, non-polar contribution to solvation.

having no significant effect on p-ERK1/2 levels (Fig. 6C-E), indicating that its anti-inflammatory effects were primarily mediated through the p38 MAPK and JNK signaling pathways. Together with previous findings from molecular docking and enrichment analyses, these *in vitro* results confirmed that quercetin alleviated synovial inflammation through coordinated regulation of MMP expression and inhibition of MAPK pathway activation, laying a mechanistic foundation for its therapeutic potential in synovitis.

Quercetin ameliorates synovitis and cartilage degradation via suppressing p38 MAPK-mediated inflammatory signaling. Multiple histological and molecular techniques, including H&E staining, Safranin O-Fast Green staining, immunofluorescence co-localization and qPCR analysis, were employed to assess quercetin's protective effects on synovial inflammation and cartilage degeneration at both tissue and molecular levels.

H&E staining results revealed that the synovial tissues of the control group exhibited normal histoarchitecture with minimal inflammation. By contrast, the CFA model group showed pronounced synovial hyperplasia and extensive infiltration of inflammatory cells. Quercetin treatment markedly reduced inflammatory cell infiltration and improved the integrity of the synovial structure (Fig. 7A). Safranin O-Fast Green staining further demonstrated a marked loss of proteoglycans in the cartilage of CFA-treated rats, as indicated by the diminished red staining. The red staining area was notably restored in the quercetin-treated group, suggesting that quercetin exerts a chondroprotective effect (Fig. 7B).

To further evaluate the molecular mechanisms underlying the anti-inflammatory effects of quercetin, dual immunofluorescence staining was performed to assess the co-localization of p-p38 MAPK with downstream inflammatory cytokines in synovial tissue. As shown in Fig. 7C, in the CFA-induced synovitis model, p-p38 MAPK was highly co-localized with IL-6 and MMP-13 in synoviocytes, with co-expression fluorescence intensities of 182.3±15.6 and 165.2±13.2, respectively. Following quercetin treatment, the co-expression intensity of p-p38 MAPK + IL-6 was significantly reduced to 122.4±12.9 in the 20 mg/kg group and 91.7±10.4 in the 40 mg/kg group ($^{*}P<0.05$ and $^{**}P<0.01$). Similarly, the co-expression of p-p38 MAPK + MMP-13 decreased to 113.5±11.7 and 85.6±9.8 at the respective doses ($^{*}P<0.05$ and $^{**}P<0.01$), indicating that quercetin effectively suppresses the co-localization of phosphorylated p38 with key inflammatory mediators in synovial tissue.

At the transcriptional level, qPCR analysis (Fig. 7D) revealed that quercetin significantly downregulated the mRNA expression of MAPK14, IL-6 and MMP13. Specifically, MAPK14 expression decreased from 3.27±0.25 in the CFA group to 1.38±0.16 in the 40 mg/kg quercetin group ($^{***}P<0.001$). Similarly, IL-6 expression was reduced from 4.01±0.33 to 1.72±0.21 and MMP13 from 3.62±0.27 to 1.45±0.19. The combined results from both tissue localization and gene expression analyses conclusively demonstrated that quercetin mediated its anti-inflammatory and chondroprotective effects through coordinated transcriptional and signaling regulation, specifically by inhibiting p38 MAPK pathway activation and consequently reducing downstream expression of inflammatory cytokines and MMPs.

In summary, quercetin alleviated synovial inflammation and subchondral bone destruction by suppressing the activation of the p38 MAPK signaling pathway and transcriptionally regulating its downstream targets, including pro-inflammatory cytokines and MMPs, in synovial tissue.

Quercetin attenuates subchondral condylar bone destruction via the p38 MAPK signaling pathway in a rat model. To further confirm whether quercetin exerts its therapeutic effects through the p38 MAPK signaling pathway, a series of *in vivo* mechanistic validations was conducted. InstantOne ELISA results (Fig. 8A) showed that the expression levels of p-p38 MAPK and p-JNK were markedly elevated in the synovial tissues of the CFA group. By contrast, quercetin

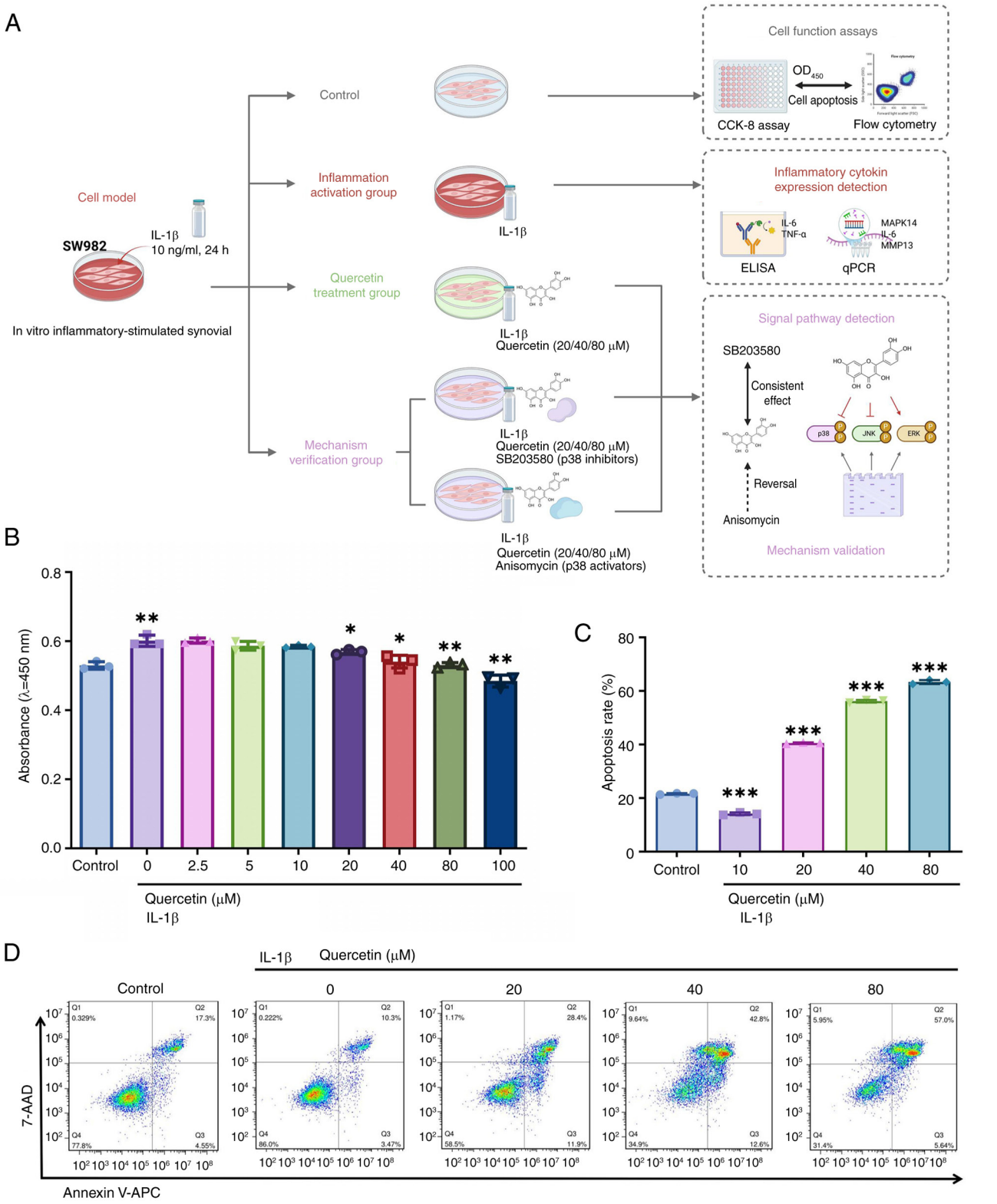

Figure 5. Evaluation of the regulatory effects of quercetin on synovial cell proliferation, apoptosis and inflammatory cytokine expression under inflammatory stimulation. (A) Schematic diagram of the *in vitro* experimental workflow. (B) CCK-8 assay showing the proliferation activity of SW982 synoviocytes after treatment with various concentrations of quercetin (0-100 μM) for 24 h. (C and D) Annexin V/7-AAD dual-staining flow cytometry analysis of apoptosis, demonstrating a concentration-dependent increase in apoptotic rate. All experiments were performed in triplicate (n=3) and data are presented as mean ± SD. Statistical comparisons between groups were conducted using one-way ANOVA. Significance levels vs. the 0 μM group are indicated as: *P<0.05, **P<0.01, ***P<0.001; ns: insignificant. CCK-8, Cell Counting Kit-8.

treatment markedly reduced p-p38 MAPK expression. IHC analysis further supported these findings (Fig. 8B), demonstrating that the expression of MMP13 and IL-6 was markedly increased in the CFA group, while quercetin treatment effectively suppressed their levels in synovial tissues. Moreover, Micro-CT analysis (Fig. 8C-E) revealed severe subchondral

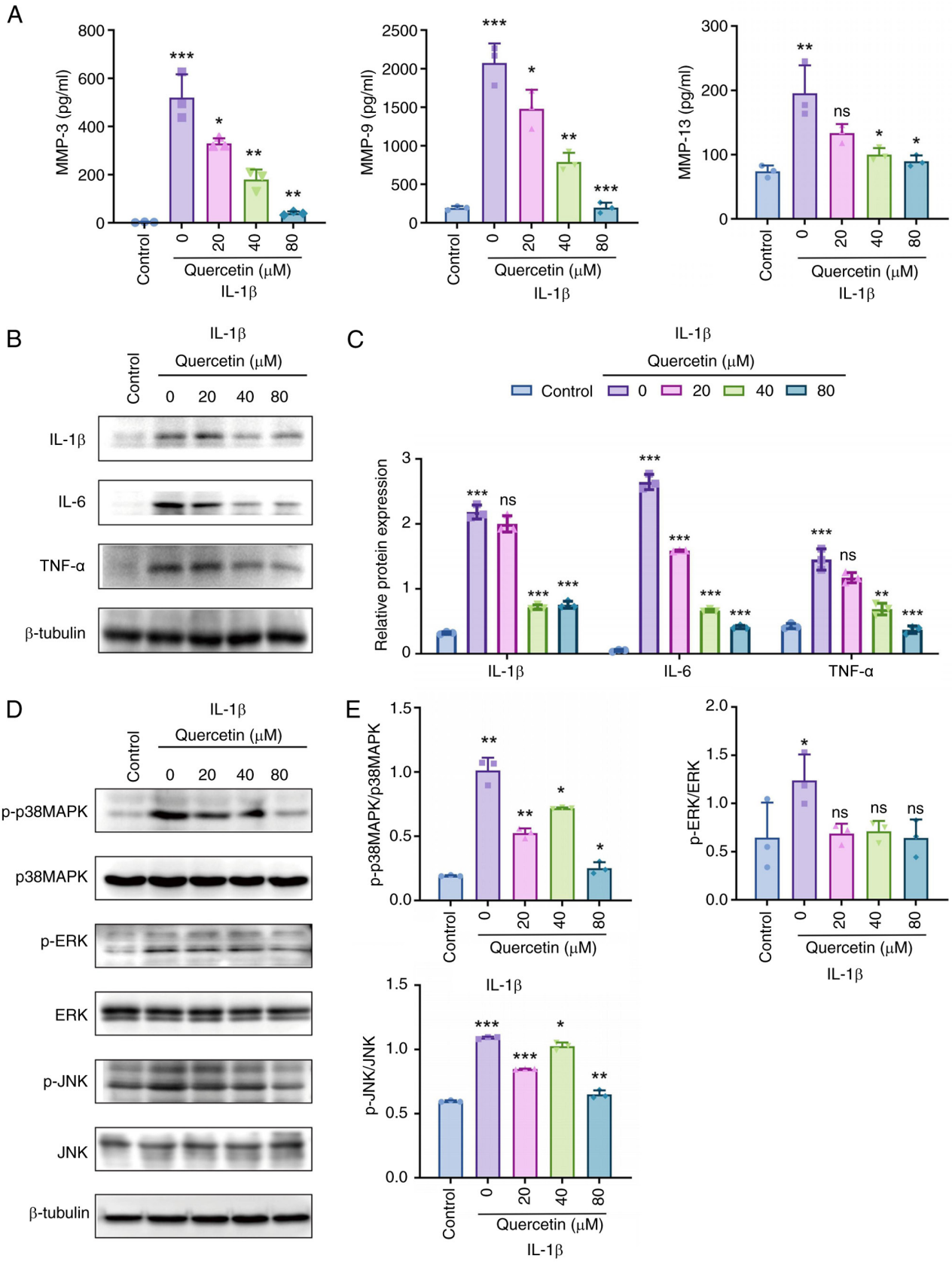

Figure 6. Multi-level validation of quercetin-mediated regulation of inflammatory cytokines and MMPs via inhibition of the p38 MAPK signaling pathway. (A) ELISA analysis showing the effects of different concentrations of quercetin on IL-1β-induced secretion of MMP3, MMP9 and MMP13 in SW982 cells; (B) Western blot analysis of TNF-α, IL-1β and IL-6 protein expression levels, with β-tubulin as the internal control; (C and D) Western blot analysis of phosphorylation levels of key MAPK signaling molecules: p38, ERK1/2 and JNK; (E) Quantitative analysis of phosphorylated proteins, showing that quercetin markedly inhibited the expression of p-p38 and p-JNK, with no significant effect on p-ERK1/2. All experiments were independently repeated three times (n=3) and data are presented as mean ± SD. Statistical comparisons were performed using one-way ANOVA. Significance levels compared with the model group or 0 μM group are indicated as: *P<0.05, **P<0.01, ***P<0.001; ns: insignificant. MMPs, matrix metalloproteinases; ELISA, enzyme-linked immunosorbent assay; p-, phosphorylated.

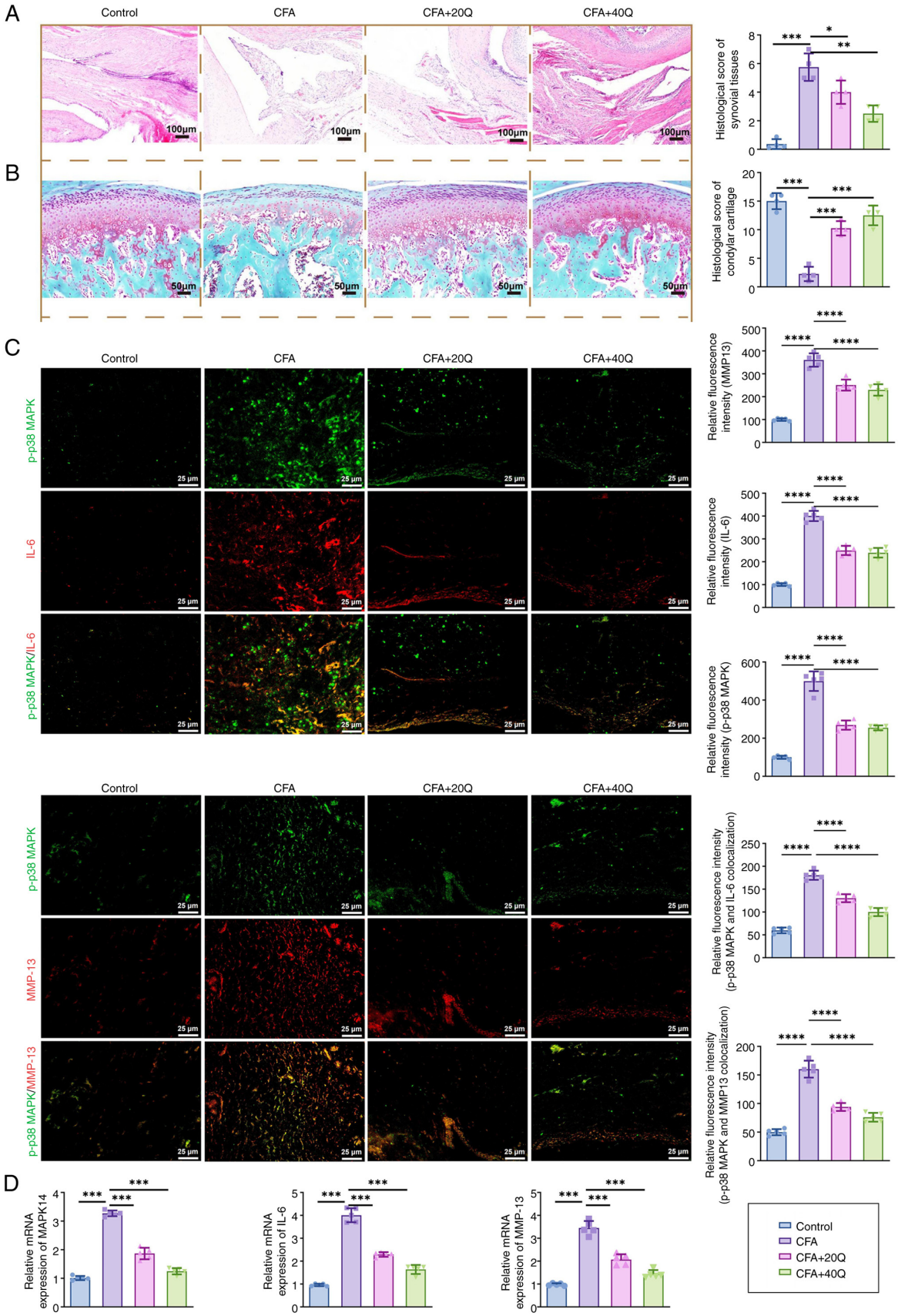

Figure 7. Multi-level analysis validates quercetin's therapeutic effects on synovitis and its regulatory role in inflammation-related signaling pathways. (A) H&E staining assessing changes in synovial structure and inflammatory cell infiltration. (B) Safranin O-Fast Green staining showing alterations in proteoglycan distribution in condylar cartilage. (C) Dual immunofluorescence staining analyzing the co-localization of p-p38 MAPK (green) with IL-6 (red) and MMP13 (red) in synovial tissue. (D) qPCR analysis of key gene expression levels, including MAPK14, MAPKAPK2, DUSP1, IL-6, TNF-α and MMP13, in SW982 cells and synovial tissues. All histological experiments were conducted with five animals per group (n=5) and molecular experiments were independently repeated three times (n=3). Data are presented as mean ± SD. Statistical comparisons were performed using one-way ANOVA. Significance levels: *P<0.05, **P<0.01, ***P<0.001, ****P<0.0001; ns, insignificant. H&E, hematoxylin and eosin; MMP, matrix metalloproteinase; qPCR, quantitative PCR.

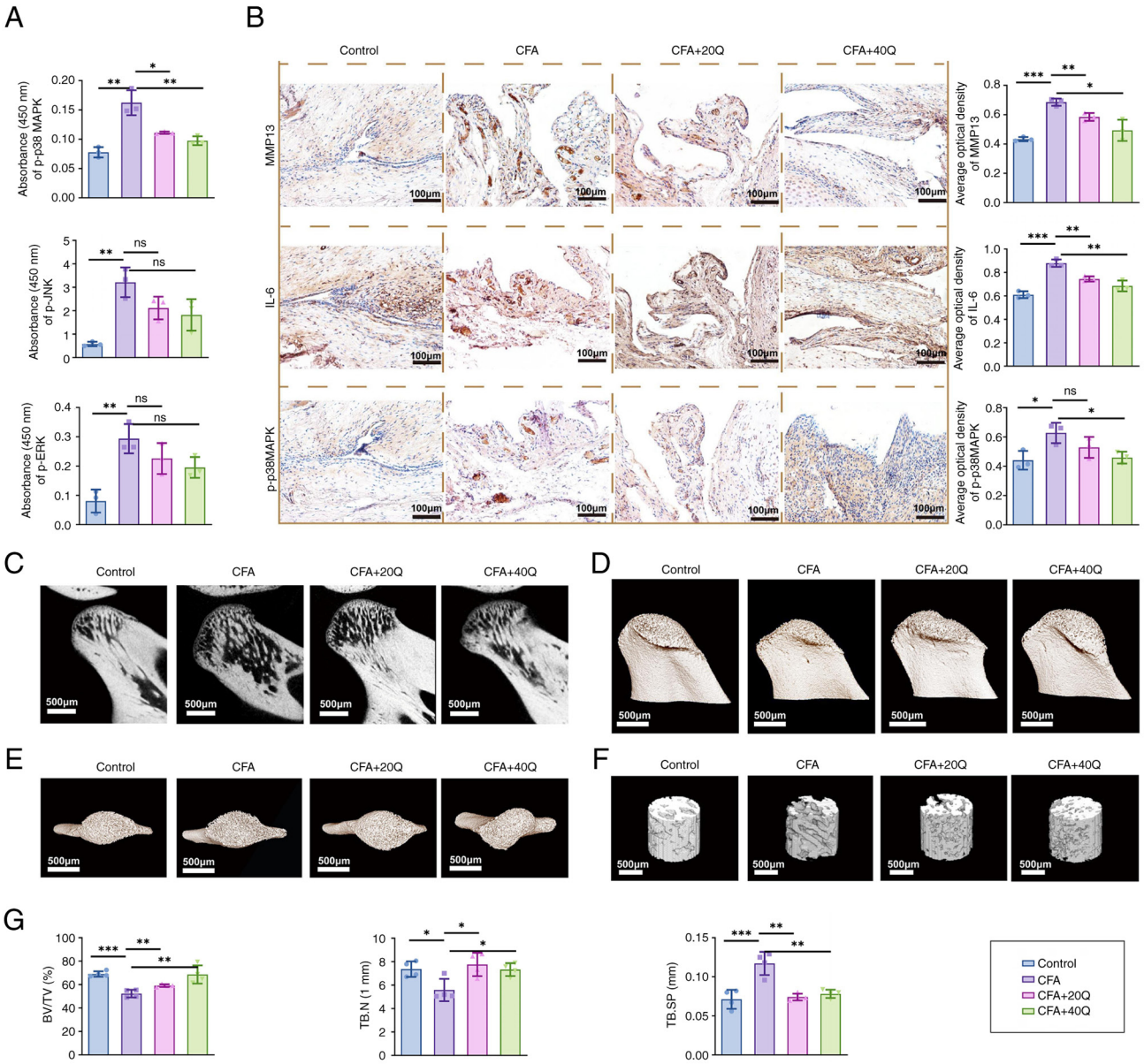

Figure 8. Quercetin alleviates inflammatory cytokine expression and mitigates bone destruction by modulating the p38 MAPK signaling pathway. (A) InstantOne ELISA analysis of p-p38 MAPK, p-JNK and p-ERK levels in synovial tissue. (B) IHC staining showing expression changes of MMP13, IL-6 and p-p38 MAPK in synovial tissue. (C) Evaluation of subchondral bone destruction using Micro-CT sagittal slices, (D and E) 3D reconstructions and (F) cylindrical ROI of rat condylar bone. (G) Quantitative analysis of BV/TV, Tb.N and Tb.Sp. Scale bar, 500 μm. Comparisons were made against the CFA group. Each group included five rats (n=5) and data are presented as mean ± SD. Statistical analysis was performed using one-way ANOVA; *P<0.05, **P<0.01, ***P<0.001. ELISA, enzyme-linked immunosorbent assay; p-, phosphorylated; IHC, immunohistochemistry; MMP, matrix metalloproteinase; Micro-CT, micro-computed tomography; ROI, region of interest; BV/TV, bone volume/tissue volume; Tb.N, trabecular number; Tb.Sp, trabecular separation; CFA, Complete Freund's Adjuvant.

bone destruction in the condylar region of CFA-treated rats, characterized by a decrease in BV/TV and Tb.N, along with an increase in Tb.Sp. Quercetin administration markedly improved all these structural parameters (Fig. 8F and 8G), indicating its protective effect on subchondral bone.

p38 MAPK agonist/inhibitor experiments confirm the signaling pathway dependency of the anti-inflammatory effect of quercetin. To further verify whether the anti-inflammatory mechanism of quercetin depends on the p38 MAPK signaling pathway, controlled experiments were conducted using both the pathway agonist anisomycin and inhibitor SB203580 in an IL-1β-stimulated SW982 synovial cell model.

As shown by western blot analysis (Fig. 9A), IL-1β stimulation markedly increased the expression level of p-p38 MAPK to 1.00±0.09 (relative grayscale value). Treatment with quercetin markedly reduced this level to 0.42±0.06 (***P<0.001). The effect of SB203580 was comparable to that of quercetin, reducing p-p38 MAPK to 0.38±0.05 (not significant vs. quercetin), indicating similar inhibitory effects. By contrast, co-treatment with the pathway agonist anisomycin partially reversed quercetin's effect, raising p-p38 MAPK levels to 0.83±0.07 (**P<0.01 vs. quercetin group). These results suggest that the anti-inflammatory effect of quercetin is, at least in part, mediated through inhibition of the p38 MAPK signaling pathway.

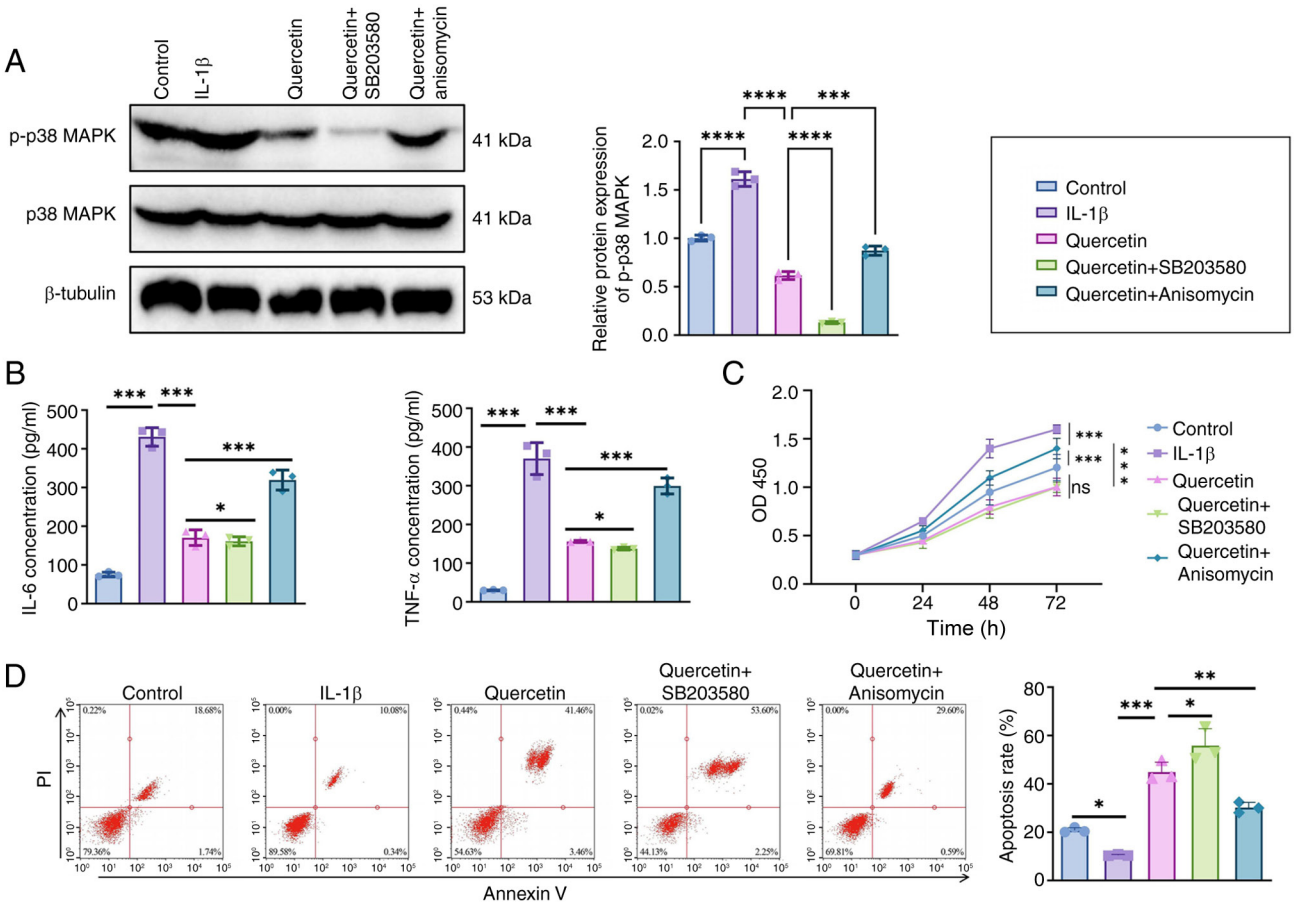

Figure 9. Agonist/inhibitor experiments confirm that the anti-inflammatory mechanism of quercetin depends on the p38 MAPK signaling pathway. (A) Western blot analysis of p-p38 MAPK protein expression. (B) ELISA detection of IL-6 and TNF-α secretion levels (pg/ml). (C) CCK-8 assay for evaluating cell proliferation activity (OD450). (D) Annexin V/PI flow cytometry analysis of apoptosis rate (%). Experimental groups included: Control, IL-1β, IL-1β + quercetin, IL-1β + quercetin + SB203580 and IL-1β + quercetin + anisomycin. All experiments were independently repeated three times (n=3) and data are expressed as mean ± SD. Statistical comparisons were performed using one-way ANOVA; *P<0.05, **P<0.01, ***P<0.001 ****P<0.0001; ns: insignificant. p-, phosphorylated; ELISA, enzyme-linked immunosorbent assay; CCK-8, Cell Counting Kit-8; OD, optical density.

ELISA results (Fig. 9B) demonstrated that IL-1β stimulation markedly increased the secretion of IL-6 and TNF-α, with levels reaching 425.6±28.4 pg/ml and 372.8±24.1 pg/ml, respectively. Quercetin treatment markedly reduced these cytokine levels to 174.2±19.3 pg/ml for IL-6 and 151.6±17.7 pg/ml for TNF-α (***P<0.001). Comparable effects were observed in the SB203580 group (IL-6: 166.5±16.4 pg/ml; TNF-α: 147.3±14.9 pg/ml; ns vs. quercetin group). However, co-treatment with the p38 MAPK agonist anisomycin led to a partial reversal, increasing IL-6 and TNF-α levels to 314.7±21.2 pg/ml and 296.5±18.3 pg/ml, respectively (**P<0.01 vs. quercetin group).

Regarding cell function, CCK-8 assay results (Fig. 9C) showed that IL-1β stimulation markedly enhanced synoviocyte proliferation, with an OD450 value of 1.62±0.07. Quercetin treatment effectively suppressed proliferation (1.09±0.06; ***P<0.001) and a similar reduction was observed in the SB203580 group (1.05±0.04; ns vs. quercetin group). Anisomycin partially reversed this inhibitory effect, increasing the OD450 value to 1.41±0.05 (**P<0.01).

Flow cytometry analysis using Annexin V/PI staining (Fig. 9D) revealed that IL-1β stimulation markedly reduced the apoptosis rate to 7.8%±1.2%. Quercetin treatment markedly increased apoptosis to 22.6%±2.1% (***P<0.001), while the SB203580 group showed a comparable increase (24.3%±1.9%). Following combined treatment with anisomycin, the apoptosis rate decreased to 12.4%±1.7% (***P<0.01 vs. quercetin group).

Taken together, these agonist/inhibitor control experiments clearly demonstrate that quercetin's anti-inflammatory, pro-apoptotic and antiproliferative effects are highly dependent on inhibiting the p38 MAPK signaling pathway, reinforcing the specificity of its underlying mechanism.

Discussion

The present study is the first, to the best of the authors' knowledge, to reveal the potential mechanism by which quercetin alleviates TMJ synovitis by inhibiting the p38 MAPK signaling pathway, thereby regulating synoviocyte inflammation and apoptosis. Quercetin markedly suppressed abnormal proliferation of synovial cells, promoted apoptosis and effectively reduced the secretion of inflammatory cytokines such as IL-6 and TNF-α. These findings not only provided new evidence for the anti-inflammatory effects of quercetin but also offered theoretical support for the critical role of the p38 MAPK signaling pathway in TMD-associated synovitis. Unlike previous studies, the present study integrated multiple experimental approaches, including molecular docking and

MD simulation, to comprehensively elucidate the mechanistic action of quercetin via the p38 MAPK pathway. Compared with conventional therapies, quercetin, as a natural compound, offers broad biological activity with fewer side effects, highlighting its promising potential for clinical application in treating TMD synovitis.

Compared with existing studies, the innovation of this research lies in its first systematic elucidation of the mechanism by which quercetin acts on TMD-associated synovitis, particularly its potential to modulate inflammation and apoptosis via the p38 MAPK signaling pathway (11). Previous studies have primarily focused on the effects of quercetin in RA and osteoarthritis, while research specifically addressing TMD synovitis remains limited. Quercetin has been demonstrated to exert anti-inflammatory effects by regulating multiple signaling pathways, such as MAPK and NF-κB (16). However, through the integration of network pharmacology and experimental validation, The present study was the first, to the best of the authors' knowledge, to propose that quercetin may alleviate TMD synovitis by inhibiting the p38 MAPK signaling pathway, thereby filling a critical gap in the current literature. Unlike conventional anti-inflammatory drugs such as NSAIDs, quercetin alleviates inflammation, modulates immune responses and protects joint integrity. These multifunctional properties highlight its broad therapeutic potential.

An unexpected finding in the present study was that quercetin markedly promotes apoptosis in synoviocytes, providing new insight into its potential application in treating TMD-associated synovitis. Consistent with previous reports on the anti-inflammatory effects of quercetin (35), the present results suggested that the pro-apoptotic effect on synovial cells may represent an additional mechanism by which quercetin alleviates inflammation in TMD synovitis. However, compared with other studies reporting varying effects of quercetin on cell proliferation under different conditions (36), the present study observed that quercetin inhibited synoviocyte proliferation and induced apoptosis at relatively low concentrations. This discrepancy may be attributed to differences in experimental conditions, including the concentration of quercetin used and the specific cell types involved. These findings warrant further investigation.

As a natural compound, quercetin possesses low toxicity and a wide range of biological activities, making its therapeutic potential in TMD-associated synovitis particularly noteworthy. Compared with conventional pharmacological treatments, quercetin offers distinct advantages in reducing inflammation, promoting synoviocyte apoptosis and facilitating the repair of subchondral bone structures (37,38). The present study demonstrated that quercetin alleviated synovitis and improved joint function by inhibiting the p38 MAPK signaling pathway. These findings suggested that quercetin may be an effective adjunctive therapy for TMD synovitis, especially for long-term management. Its natural origin and low risk of adverse effects make it an ideal candidate for chronic treatment in patients with TMD. In the future, quercetin may also be combined with other anti-inflammatory agents to enhance therapeutic efficacy while reducing long-term drug dependence in patients, offering a promising strategy for integrated, low-toxicity management of TMD-related joint inflammation.

Although the present study established a relatively comprehensive mechanistic framework across multiple levels, several limitations should be acknowledged. First, SW982 cells were used as the sole representative of synoviocytes, without including primary synovial cells or different synovial subtypes under varying inflammatory conditions. Second, while the study highlighted the role of the p38 MAPK signaling pathway, it did not further explore the potential crosstalk with other key inflammatory pathways, such as JNK or NF-κB. Additionally, the long-term effects of quercetin in chronic TMD models have yet to be evaluated. Lastly, systematic pharmacokinetic and toxicological assessments were not conducted in the present study and future research is needed to address these aspects to ensure quercetin's clinical safety and applicability.

Future research may further explore the interplay between signaling pathways, particularly the synergistic regulatory mechanisms between the p38 MAPK signaling pathway and other inflammation-related pathways. To enhance the physiological relevance of *in vitro* experiments, primary synoviocytes or 3D organoid models should be considered. Additionally, establishing chronic TMD animal models would allow for evaluating quercetin's long-term therapeutic efficacy and potential to prevent disease recurrence. Further studies should also focus on drug delivery strategies by developing quercetin-based targeted delivery systems, such as microspheres or nanocarriers, to improve its bioavailability. Finally, comprehensive safety assessments and preclinical pharmacodynamic evaluations are essential to support future clinical translation and provide a solid foundation for clinical trials.

The present study is the first, to the best of the authors' knowledge, to elucidate the potential mechanism by which quercetin alleviates TMD-associated synovitis by inhibiting the p38 MAPK signaling pathway, thereby regulating synoviocyte inflammation and apoptosis. As a natural compound, quercetin offers a novel therapeutic strategy for TMD due to its anti-inflammatory properties and low toxicity profile. Although certain limitations exist in the present study, quercetin's multiple biological activities and favorable safety characteristics highlight its promise as a candidate drug for treating TMD synovitis. Future research should further validate its clinical efficacy and investigate its potential in combination therapies, promoting its broader application in TMD and other inflammation-related disorders.

The present study systematically integrated network pharmacology, molecular simulations, *in vitro* cellular assays and *in vivo* animal models to elucidate, for the first time, to the best of the authors' knowledge, the mechanism by which quercetin alleviates TMJ synovitis. The results demonstrated that quercetin exerted its effects by targeting the p38 MAPK signaling pathway, markedly reducing its phosphorylation level. This inhibition led to the downregulation of inflammatory cytokines such as IL-6, TNF-α and MMPs, thereby attenuating synovial inflammation, promoting synoviocyte apoptosis and protecting the subchondral bone structure. The functional verification using a p38 MAPK pathway agonist and inhibitor confirms that these effects depend highly on p38 MAPK activity. The present study uncovered the multi-target anti-inflammatory mechanism of quercetin and provides experimental evidence supporting the role of the p38 MAPK signaling pathway in TMD-related synovitis.

Acknowledgements

Not applicable.

Funding

The present study was supported by the National Natural Science Foundation of China (grant no. 82370987).

Availability of data and materials

The data generated in the present study are included in the figures and/or tables of this article.

Authors' contributions

XY and YL conceived and designed the study. MC, YG and XX performed the experiments. YG, XX and XY analyzed the data. MC and XX wrote the manuscript. XY and YL confirm the authenticity of all the raw data. All authors reviewed and approved the final version of the manuscript.

Ethics approval and consent to participate

All experimental procedures were approved by the Animal Ethics Committee of China Medical University (approval no. kt2022112) and conducted by institutional guidelines.

Patient consent for publication

Not applicable.

Competing interests

The authors declare that they have no competing interests.

References

1. Kapos FP, Exposto FG, Oyarzo JF and Durham J: Temporomandibular disorders: A review of current concepts in aetiology, diagnosis and management. Oral Surg 13: 321-334, 2020.
2. Zieliński G, Pająk-Zielińska B and Ginszt M: A meta-analysis of the global prevalence of temporomandibular disorders. J Clin Med 13: 1365, 2024.
3. Zieliński G: Quo vadis temporomandibular disorders? By 2050, the global prevalence of TMD may approach 44%. J Clin Med 14: 4414, 2025.
4. Li DTS and Leung YY: Temporomandibular disorders: Current concepts and controversies in diagnosis and management. Diagnostics (Basel) 11: 459, 2021.
5. Wang XD, Zhang JN, Gan YH and Zhou YH: Current understanding of pathogenesis and treatment of TMJ osteoarthritis. J Dent Res 94: 666-673, 2015.
6. Gil-Martinez A, Paris-Alemany A, López-de-Uralde-Villanueva I and La Touche R: Management of pain in patients with temporomandibular disorder (TMD): challenges and solutions. J Pain Res 11: 571-587, 2018.
7. Andre A, Kang J and Dym H: Pharmacologic treatment for temporomandibular and temporomandibular joint disorders. Oral Maxillofac Surg Clin North Am 34: 49-59, 2022.
8. Tamer TM: Hyaluronan and synovial joint: Function, distribution and healing. Interdiscip Toxicol 6: 111-125, 2013.
9. Jerosch J: Effects of glucosamine and chondroitin sulfate on cartilage metabolism in OA: Outlook on other nutrient partners especially omega-3 fatty acids. Int J Rheumatol 2011: 1-17, 2011.
10. Wujec M and Feldo M: Can we improve diosmetin activity? The state-of-the-art and promising research directions. Molecules 28: 7910, 2023.
11. Sun Z, Liu K, Liang C, Wen L, Wu J, Liu X and Li X: Diosmetin as a promising natural therapeutic agent: In vivo, in vitro mechanisms, and clinical studies. Phytother Res 38: 3660-3694, 2024.
12. Aghababaei F and Hadidi M: Recent advances in potential health benefits of quercetin. Pharmaceuticals (Basel) 16: 1020, 2023.
13. Wang G, Wang Y, Yao L, Gu W, Zhao S, Shen Z, Lin Z, Liu W and Yan T: Pharmacological activity of quercetin: An updated review. Evid Based Complement Alternat Med 2022: 1-12, 2022.
14. Silva-Pinto PA, de Pontes JTC, Aguilar-Morón B, Canales CSC, Pavan FR and Roque-Borda CA: Phytochemical insights into flavonoids in cancer: Mechanisms, therapeutic potential, and the case of quercetin. Heliyon 11: e42682, 2025.
15. Shabir I, Kumar Pandey V, Shams R, Dar AH, Dash KK, Khan SA, Bashir I, Jeevarathinam G, Rusu AV, Esatbeyoglu T and Pandiselvam R: Promising bioactive properties of quercetin for potential food applications and health benefits: A review. Front Nutr 9: 999752, 2022.
16. Ding H, Ding H, Mu P, Lu X and Xu Z: Diosmetin inhibits subchondral bone loss and indirectly protects cartilage in a surgically-induced osteoarthritis mouse model. Chem Biol Interact 370: 110311, 2023.
17. Zhao L, Zhang H, Li N, Chen J, Xu H, Wang Y and Liang Q: Network pharmacology, a promising approach to reveal the pharmacology mechanism of Chinese medicine formula. J Ethnopharmacol 309: 116306, 2023.
18. Zhang P, Zhang D, Zhou W, Wang L, Wang B, Zhang T and Li S: Network pharmacology: Towards the artificial intelligence-based precision traditional Chinese medicine. Brief Bioinform 25: bbad518, 2023.
19. Bhoi A, Dwivedi SD, Singh D, Keshavkant S and Singh MR: Mechanistic prospective and pharmacological attributes of quercetin in attenuation of different types of arthritis. 3 Biotech 13: 362, 2023.
20. Yang Y, Kim SC, Yu T, Yi YS, Rhee MH, Sung GH, Yoo BC and Cho JY: Functional roles of p38 mitogen-activated protein kinase in macrophage-mediated inflammatory responses. Mediator Inflamm 2014: 1-13, 2014.
21. Kim AL, Labasi JM, Zhu Y, Tang X, McClure K, Gabel CA, Athar M and Bickers DR: Role of p38 MAPK in UVB-induced inflammatory responses in the skin of SKH-1 hairless mice. J Invest Dermatol 124: 1318-1325, 2005.
22. Sui X, Kong N, Ye L, Han W, Zhou J, Zhang Q, He C and Pan H: p38 and JNK MAPK pathways control the balance of apoptosis and autophagy in response to chemotherapeutic agents. Cancer Lett 344: 174-179, 2014.
23. Mathiessen A and Conaghan PG: Synovitis in osteoarthritis: Current understanding with therapeutic implications. Arthritis Res Ther 19: 18, 2017.
24. Bartels YL, van Lent PLEM, van der Kraan PM, Blom AB, Bonger KM and van den Bosch MHJ: Inhibition of TLR4 signalling to dampen joint inflammation in osteoarthritis. Rheumatology (Oxford) 63: 608-618, 2023.
25. Chin CH, Chen SH, Wu HH, Ho CW, Ko MT and Lin CY: CytoHubba: Identifying hub objects and sub-networks from complex interactome. BMC Syst Biol 4: S4-S11, 2014.
26. Bayly CI, Cieplak P, Cornell W and Kollman PA: A well-behaved electrostatic potential based method using charge restraints for deriving atomic charges: The RESP model. J Phys Chem 97: 10269-10280, 1993.
27. Jorgensen WL, Chandrasekhar J, Madura JD, Impey RW and Klein ML: Comparison of simple potential functions for simulating liquid water. J Chem Phys 79: 926-935, 1983.
28. Zakrzewska M, Opalinski L, Haugsten EM, Otlewski J and Wiedlocha A: Crosstalk between p38 and Erk 1/2 in downregulation of FGF1-induced signaling. IJMS 20: 1826, 2019.
29. Mei S, Gu H, Ward A, Yang X, Guo H, He K, Liu Z and Cao W: p38 Mitogen-activated protein kinase (MAPK) promotes cholesterol ester accumulation in macrophages through inhibition of macroautophagy. J Biol Chem 287: 11761-11768, 2012.
30. National Research Council (US) Committee for the Update of the Guide for the Care and Use of Laboratory Animals: Guide for the Care and Use of Laboratory Animals, 8th edition. National Academies Press (US), Washington, DC, 2011.

31. Hu S, Li H, Jiang H, Liu X, Ke J and Long X: Macrophage activation in synovitis and osteoarthritis of temporomandibular joint and its relationship with the progression of synovitis and bone remodeling. Am J Pathol 194: 296-306, 2024.
32. Livak KJ and Schmittgen TD. Analysis of relative gene expression data using real-time quantitative PCR and the 2(-Delta Delta C(T)) method. Methods 25: 402-408, 2001.
33. Gynther GW, Dijkgraaf LC, Reinholt FP, Holmlund AB, Liem RS, and de Bont LG: Synovial inflammation in arthroscopically obtained biopsy specimens from the temporomandibular joint: A review of the literature and a proposed histologic grading system. J Oral Maxillofac Surg 56: 1281-1286, 1998.
34. Cheng M, Yi X and Zhou Q: Overexpression of HIF-1alpha in bone marrow mesenchymal stem cells promote the repair of mandibular condylar osteochondral defect in a rabbit model. J Oral and Maxillofacial Surgery 79: 345.e1-345.e15, 2021.
35. Chen Y, Wang Y, Liu M, Zhou B and Yang G: Diosmetin exhibits anti-proliferative and anti-inflammatory effects on TNF-α-stimulated human rheumatoid arthritis fibroblast-like synoviocytes through regulating the Akt and NF-κB signaling pathways. Phytotherapy Research 34: 1310-1319, 2019.
36. Guo G and Dong J: Diosmetin attenuates oxidative stress-induced damage to lens epithelial cells via the mitogen-activated protein kinase (MAPK) pathway. Bioengineered 13: 11072-11081, 2022.
37. Li Y, Yao J, Han C, Yang J, Chaudhry MT, Wang S, Liu H and Yin Y: Quercetin, inflammation and immunity. Nutrients 8: 167, 2016.
38. Cheng S, Gao N, Zhang Z, Chen G, Budhraja A, Ke Z, Son YO, Wang X, Luo J and Shi X: Quercetin induces tumor-selective apoptosis through downregulation of Mcl-1 and activation of bax. Clin Cancer Res 16: 5679-5691, 2010.